UCLA

Structural & Geotechnical Engineering Laboratory

Full Scale Cyclic Testing of Foundation Support Systems for Highway Bridges. Part II: Abutment Backwalls

PRINCIPAL INVESTIGATOR
Jonathan P. Stewart
University of California, Los Angeles

CO-PRINCIPAL INVESTIGATORS
Ertugrul Taciroglu and John W. Wallace
University of California, Los Angeles

GRADUATE STUDENTS
Eric R. Ahlberg, Anne Lemnitzer, Changsoon Rha, and Payman K. Tehrani
University of California, Los Angeles

STAFF OF NEES@UCLA
Steve Keowen, Robert L. Nigbor and Alberto Salamanca
University of California, Los Angeles

A report on research conducted under Grant No. 59A0247
from the California Department of Transportation

Report

Department of Civil and Environmental Engineering
University of California, Los Angeles

October 2007

UCLA - SGEL
Report 2007/02

Full Scale Cyclic Testing of Foundation Support Systems for Highway Bridges. Part II: Abutment Backwalls

Full Scale Cyclic Testing of Foundation Support Systems for Highway Bridges. Part II: Abutment Backwalls

PRINCIPAL INVESTIGATOR

Jonathan P. Stewart
University of California, Los Angeles

CO-PRINCIPAL INVESTIGATORS

Ertugrul Taciroglu and John W. Wallace
University of California, Los Angeles

GRADUATE STUDENTS

Eric R. Ahlberg, Anne Lemnitzer, Changsoon Rha, and Payman K. Tehrani
University of California, Los Angeles

STAFF OF NEES@UCLA

Steve Keowan, Robert L. Nigbor and Alberto Salamanca
University of California, Los Angeles

A report on research conducted under Grant No. 59A0247
from the California Department of Transportation

Report

Department of Civil and Environmental Engineering
University of California, Los Angeles
October 2007

Table of Contents

List of Figures

List of Tables

Acknowledgments

Support for this research was provided by the California Department of Transportation under Research Contract No. 59A0247 (and amendments thereto), which is gratefully acknowledged. We would like to acknowledge the valuable assistance and technical support of Caltrans staff in this project, particularly Anoosh Shamsabadi and Craig Whitten. George Cooke of GB Cooke Inc is recognized for his assistance in specimen construction and contract administration.

The authors gratefully acknowledge that this research was conducted with equipment purchased and integrated into the NEES@UCLA Equipment Site with support from NSF Cooperative Agreement CMS-0086596. The assistance provided by NEES@UCLA System Administrator Steve Kang and NEES System Integration team member Mr. Paul Hubbard was greatly appreciated.

Executive Summary

This research involved analysis and field testing of numerous foundation support components for highway bridges. Two classes of components were tested - cast-in-drilled-hole (CIDH) reinforced concrete piles (drilled shafts) and an abutment backwall. The emphasis of this document (Part II of the full report) is abutment backwall elements.

The backwall test specimen was backfilled to a height of 5.5 up from the base of the wall with well-compacted silty sand backfill material (SE 30). The wall is displaced perpendicular to its longitudinal axis. Wing walls are constructed with low-friction interfaces to simulate 2D conditions. The backfill extends below the base of the wall to ensure that the failure surface occurs entirely within the sand backfill soil, which was confirmed following testing. The specimen was constructed and tested under boundary conditions in which the wall was displaced laterally into the backfill and not allowed to displace vertically.

A maximum passive capacity of 490 kips was attained at a wall displacement of about 2.0 in, which corresponds to a passive earth pressure coefficient K_p of 17.6. Strain softening occurs following the peak resistance, and a residual resistance of approximately 450 kips is achieved for displacements > 3.0 inch. The equivalent residual passive earth pressure coefficient is K_p = 15.6 and the equivalent uniform passive pressure at residual is approximately 5.5 ksf, which is larger than the value in the 2004 Seismic Design Criteria of 5.0 ksf. The average abutment stiffness K_{50} was defined as a secant stiffness through the origin and the point of 50% of the ultimate passive force. For an abutment wall with a backfill height H of 5.5 ft, this stiffness was found to be K_{50} = 50 kip/in per foot of wall. The load-deflection behavior of the wall-backfill system is reasonably well described by a hyperbolic curve, which can be written using a number of formulations in the literature.

The passive pressure resultant is under predicted using classical Rankine or Coulomb earth pressure theories, whereas the log-spiral formulation over-predicts. The best estimate of capacity was obtained using a method-of-slices. This method-of-slices, as implemented with the log-spiral hyperbolic method of evaluating backbone curves, also provides a reasonable estimate of the shape of the observed load-deflection relationship.

1 INTRODUCTION

Bridge structures are typically constructed with earth abutments at their ends. As show in Figure 1.1, typical components of seat type bridge abutments in current California design practice include a backwall, two wingwalls, a support foundation (spread footings or piles) and the retained soil. The behavior of the backwall when struck by a bridge deck displacing longitudinally during earthquake shaking is a significant, yet poorly understood, aspect of bridge design. Lam and Martin (1986) described abutment performance as the "largest unknown in the area of bridge foundations." Arguably, this remains true today, despite significant progress in recent years in the testing and simulation of abutment performance. In this report, we describe the state of knowledge regarding abutment performance from both analytical and experimental perspectives. We will present the results of a field experiment to investigate abutment performance under a prescribed set of boundary conditions that is very practical for Caltrans seismic design practice, as well as the results of post-test analysis of the test data.

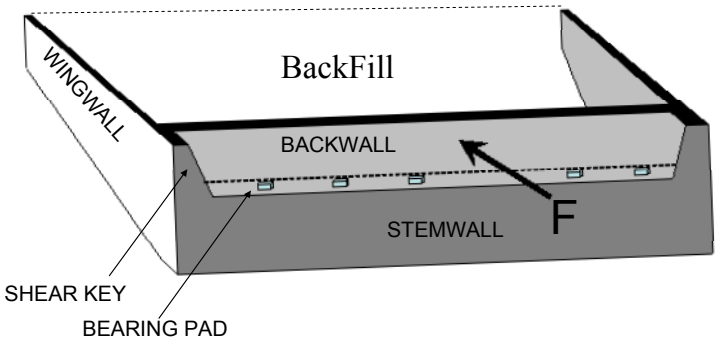

Figure 1.1.Typical configuration of bridge abutment showing major components

Abutment backwalls are designed to break away from their foundations when struck by the bridge deck and to displace in the longitudinal direction. The current experiment considers an abutment backwall that rests unanchored on natural soil. Accordingly, the test focuses on the

deformation and strength behavior of the backfill soil, which is a compacted silty sand. The wall is displaced longitudinally into the backfill, which is the deformed state illustrated on the left side of Figure 1.2. The other boundary conditions shown in Figure 1.2 are not common modes of displacement for backwalls. In our test, the backwall displaces between simulated wingwalls parallel to the direction of wall displacement (Figure 1.1).

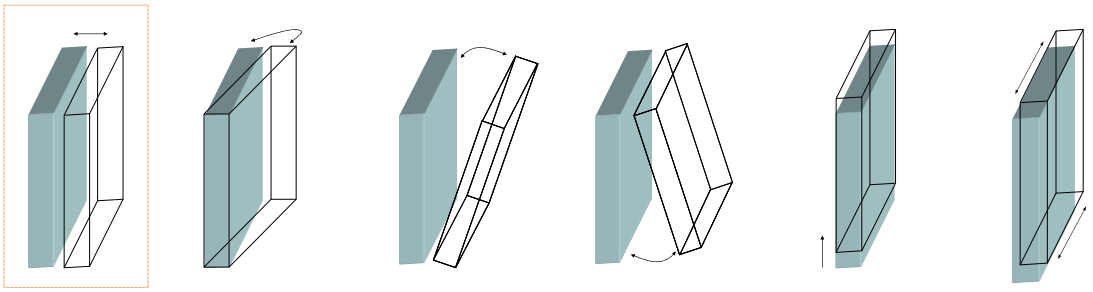

Figure 1.2. Wall displacement modes relative to backfill. The condition applied in the present testing is shown in the left frame.

Following this introduction, this report reviews in Chapter 2 previous (and ongoing) research on abutment walls. A focus of the discussion is on the load-deflection behavior and ultimate capacity of retaining structures under passive conditions. Chapter 3 introduces the test set-up, sensor layout, and control system (which includes software specifically developed to enforce the deformed state depicted in Figure 1.2). The full scale specimen, including the wall and backfill soil, is described in Chapter 4. The test protocol and results are presented in Chapter 5. Also described in Chapter 5 is the degree to which the intended boundary conditions were realized. Chapter 6 investigates the soil failure observed during the test, providing documentation on the position of the passive wedge and the soil failure surface. The results of the test are compared in Chapter 7 to analytical predictions made using the models from Chapter 2.

2 LITERATURE REVIEW

When a backwall is displaced into its backfill soil, the principal source of resistance to lateral displacement is provided by the shear resistance within the backfill. The ultimate capacity of the backwall is achieved when the soil is in a state of passive earth pressure. Three classical methods have been used to estimate passive earth pressures: Coulomb (1776), Rankine (1857), and Terzaghi (1943). Recent research has focused on (1) load-deflection modeling of abutment walls up to the point of passive failure and (2) testing of wall-soil systems in the field or laboratory, and comparing the data to analytical predictions.

2.1 Passive Earth Pressures – Ultimate Values

Coulomb Method

One of the earliest methods for estimating earth pressures against walls is credited to Coulomb (1776). As shown in Figure 2.1, Coulomb assumed the soil failure to occur in the form of a wedge undergoing translation as a rigid body along a shear plane. His theory treats the soil as isotropic and accounts for both internal friction and friction at the wall-soil interface (friction angle δ).

The passive pressure resultant force based on Coulomb theory is:

$$P_p = \frac{1}{2} K_p \gamma H^2 \tag{2.1}$$

where P_p = passive earth pressure resultant force

K_p = coefficient of passive earth pressure

γ = unit weight of the backfill soil

H = height of the wall.

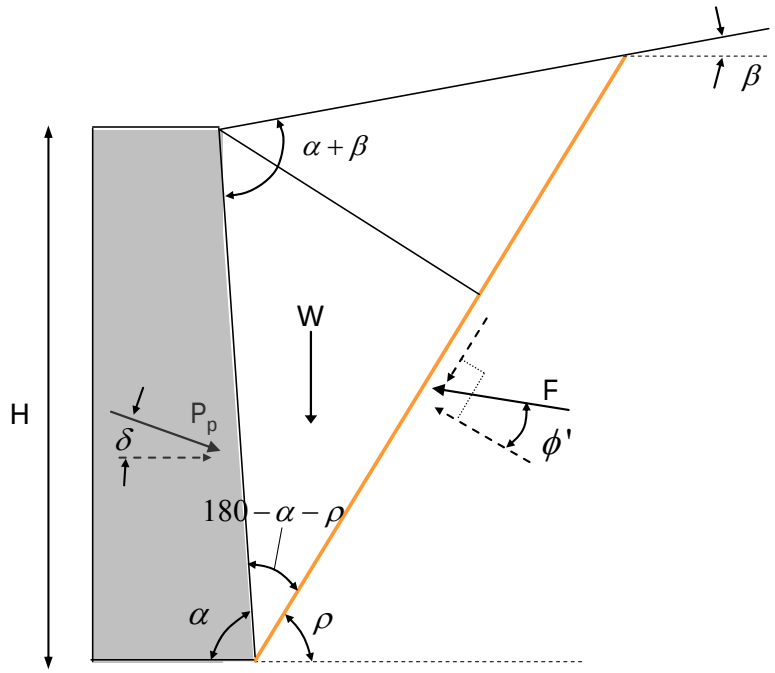

Figure 2.1. Schematic forces acting on a retaining/abutment wall

By iterating on the rupture surface angle (ρ) that minimizes K_p, the following expression for K_p can be derived using the system geometric parameters from Figure 2.1:

$$K_p = \frac{\sin^2(\alpha - \phi)}{\sin^2 \alpha \sin(\alpha + \delta)\left[1 + \sqrt{\frac{\sin(\phi + \delta)\sin(\phi + \beta)}{\sin(\alpha + \delta)\sin(\alpha + \beta)}}\right]^2} \tag{2.2}$$

where β = angle between backfill surface lines and a horizontal line (see Figure 2.1)

ϕ' = drained friction angle of the backfill soil

α angle between a horizontal line and the back face of the wall

δ = angle of wall friction.

The variation of K_p with respect to the shear strength of the backfill soil and geometric characteristics of the wall-soil system are well documented (e.g., Salgado, 2006; US Navy, 1982). In the case of zero friction at the wall-soil interface, a vertical back face, zero backfill cohesion, and a horizontal backfill surface (α=90, β=0, δ=0), the passive pressure coefficient K_p reduces to

$$K_p = \frac{1+\sin\phi'}{1-\sin\phi'} = \tan^2(45+\frac{\phi'}{2}) \tag{2.3}$$

The passive earth pressure acting against the wall (σ'_p), for a granular backfill, is computed as;

$$\sigma'_p = \sigma'_0 K_p = \gamma z \tan^2(45+\frac{\phi'}{2}) \tag{2.4}$$

where z = depth within the backfill soil.

Rankine Method

The Rankine (1857) method of evaluating passive pressure is a special case of the conditions considered by Coulomb. In particular, Rankine assumes that there is no friction at the wall-soil interface ($\delta = 0$). The coefficient of Rankine's passive earth pressure can be computed as:

$$K_p = \frac{\cos\beta + \sqrt{[\cos^2\beta - \cos^2\phi]}}{\cos\beta - \sqrt{[\cos^2\beta - \cos^2\phi]}} \tag{2.5}$$

When the embankment slope angle β equals zero, K_p from Eq. 2.5 reduces to what is shown in Eq. 2.3.

Log Spiral Method

Terzaghi (1943) extended the Coulomb earth pressure theory to accommodate a failure surface geometry consisting of log-spiral and linear segments as depicted in Figure 2.2. As with the Coulomb method, the geometry of the critical failure surface is established through a minimization of the passive earth pressure force required to maintain equilibrium with the soil at failure along the shear surface. The passive earth pressure force location at the face of the wall is pre-selected depending on the backfill type. In example, with cohesionless soils P_p is assumed to be located at 1/3 of the wall height up from the base of the wall. Results of the minimization problem, expressed in terms of the variables defined in Figure 2.2, are presented in Figure 2.3. While the coefficient of active earth pressure K_a can be read directly from the graph, K_p needs to be multiplied by a reduction factor R (shown at the top of Figure 2.3). Using K_p values from Figure 2.3, the passive earth pressure resultant force can be calculated using Eq. 2.1. The Terzaghi solution provides lower K_p values than Coulomb for wall-soil interface friction values $\delta > \phi/3$. The log spiral shape of the failure plane has generally been borne out by experiments, and hence the Terzaghi solution is generally preferred over that of Coulomb.

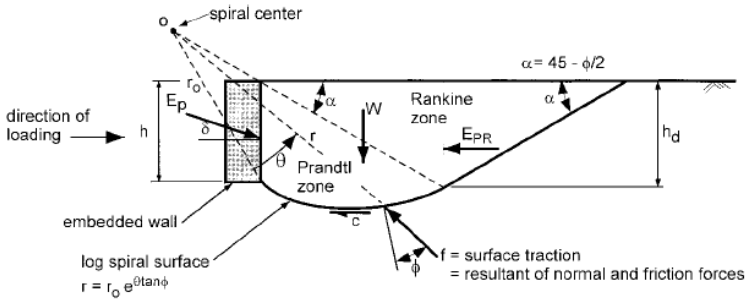

Figure 2.2. Log spiral failure mechanism after Terzaghi (Duncan and Mokwa, 2001)

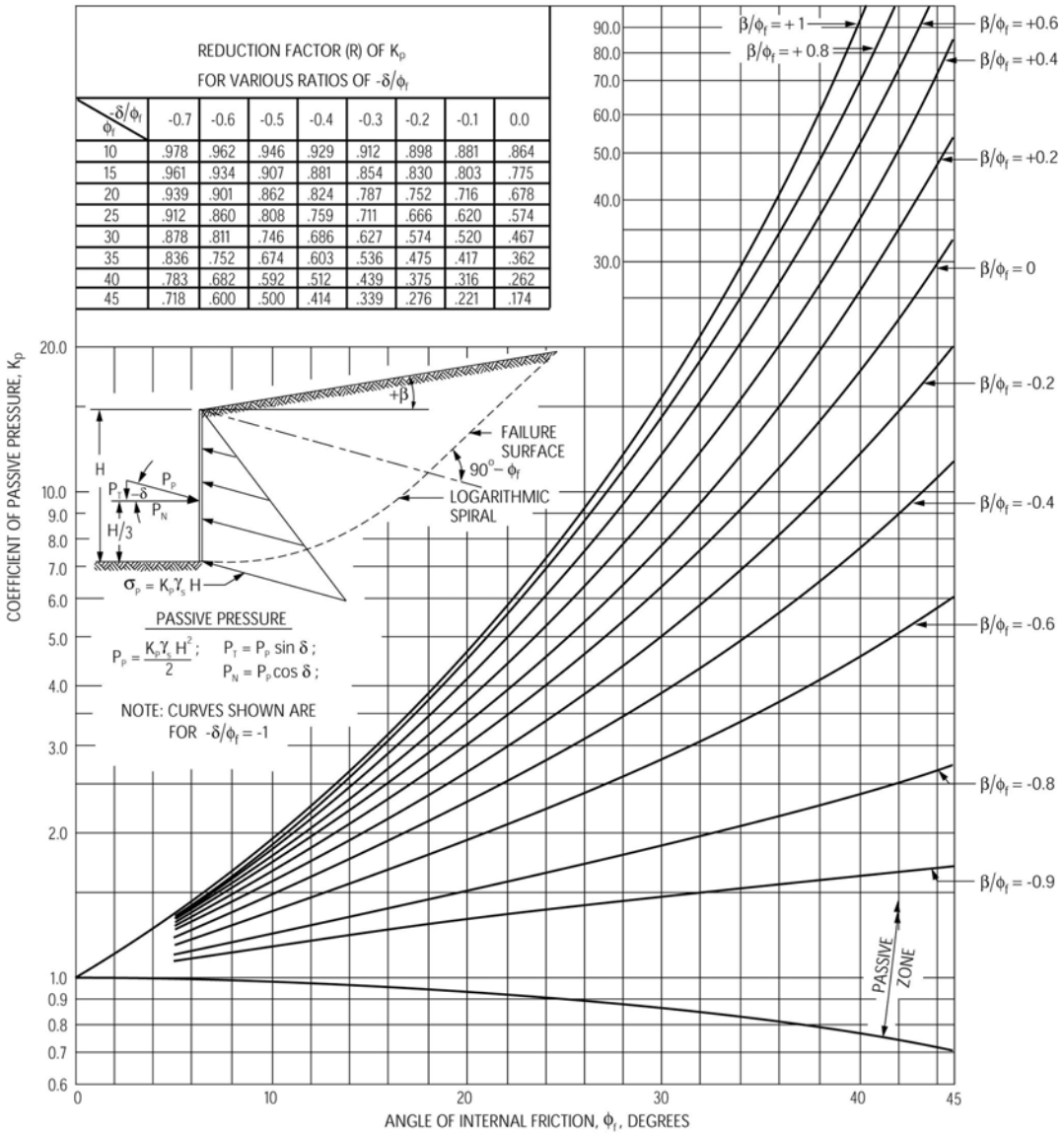

Figure 2.3. Coefficients for active and passive earth pressure using log spiral method (Caquot and Kerisel 1948)

Method of slices

The log-spiral method of Terzaghi (1943) can be extended using the method of slices to calculate the passive pressure resultant. Janbu (1957) used a method of slices with bearing capacity factors to calculate passive pressure resultants. This work was extended by Shields and Tolunay (1973) for the case of a vertical wall and horizontal cohesionless backfill using Bishop's modified method in which inter-slice shear forces are assumed to be zero (causing the passive pressure resultant to be underestimated). Shamsabadi et al. (2005 and 2007) extended this previous work by considering both horizontal and vertical inter-slice forces *(E_{ij}* and T_{ij} as shown in Figure 2.4) and linking pre-failure mobilized stresses to strains (through a hyperbolic stress-strain relationship) to calculate the displacement response. Shamsabadi et al. (2005 and 2007) do not assume the inter-slice shear forces (T_{ij}) but calculates them as part of the solution process. The mobilized abutment-soil friction angle (δ_m) of each slice is a function of the stress level in the soil and the friction angle δ at failure. The solution can be applied to cohesionless as well as cohesive backfill soils. No a priori assumption of the location of the passive resultant force is made.

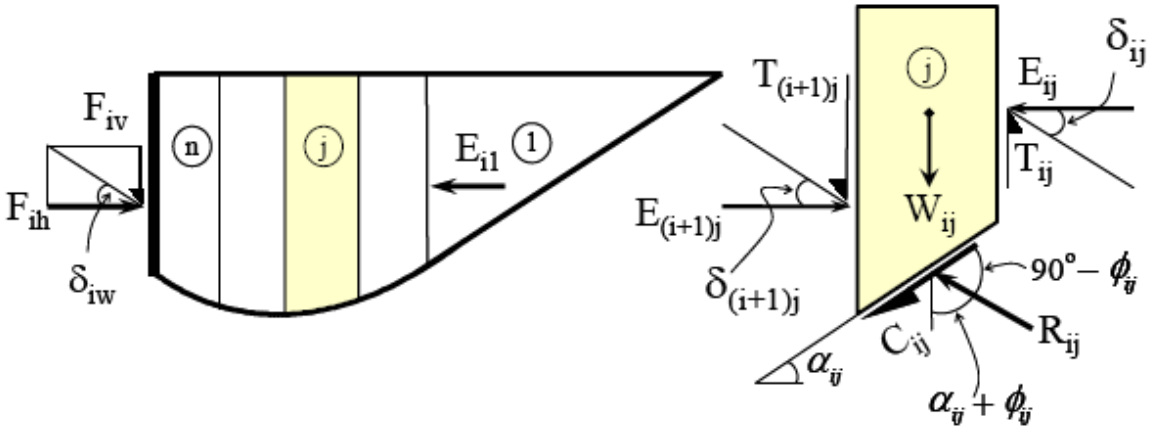

Figure 2.4. Forces on mobilized logarithmic-spiral passive wedge (Shamsabadi et al., 2007)

2.2 Load–Deflection Relationships of Wall-Soil System

Models Based on Hyperbolic Stress-Strain Relationship for Soil

Hyperbolic models have long been used to approximate load-deflection and stress-strain relationships for problems in soil mechanics (Duncan and Chang, 1970). A number of investigators have adapted various forms of hyperbolic models to simulate the load-deflection behavior of retaining walls pushed into backfill. The basic form of the hyperbolic model can be written as:

$$P = \frac{y}{A + By} \tag{2.6}$$

where P = lateral force on retaining wall corresponding to lateral deflection y, and A and B are constants that are determined differently in different forms of the hyperbolic model.

Duncan and Mokwa (2001) introduced the use of a hyperbolic equation for load-deflection modeling of retaining structures. The parameters describing their hyperbolic model are shown in Figure 2.5 and in the equation below:

$$P = \frac{y}{\frac{1}{K_{\max}} + R_f \frac{y}{P_{ult}}} \tag{2.7}$$

Hence, $A = 1/K_{max}$ and $B = R_f/P_{ult}$. As shown in Figure 2.5, K_{max} = initial stiffness (force/length), P_{ult} = ultimate passive resistance (calculated using formulations in Section 2.1) and R_f = failure ratio (= P_{ult}/hyperbolic asymptote). K_{max} is estimated using the theory of elasticity, and depends on the dimensions of the wall and elastic properties such as Youngs modulus and Poisson's ratio. R_f is an empirical constant, which Duncan and Mokwa (2001) indicate can be estimated as 0.85.

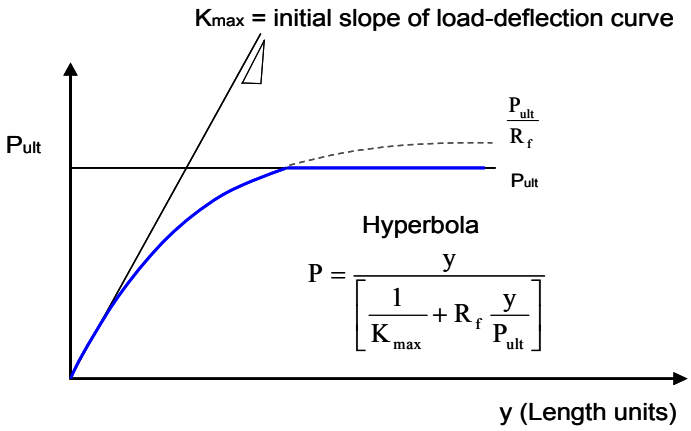

Figure 2.5. Hyperbolic load deflection relationship used by Duncan and Mowka (2001)

An alternative approach for describing a hyperbolic load-deflection relationship that is sometimes used in practice is represented in Fig. 2.6. Instead of using the initial slope of the load displacement curve, the average abutment stiffness K_{50} is calculated as the secant stiffness through the origin and the point at a force level of 50% of ultimate ($0.5P_{ult}$). The displacement at this force level is denoted y_{50}. Parameters A and B from Eq. 2.6 can be expressed in terms of y_{50}, $0.5P_{ult}$, y_{max}, and P_{ult} as follows Shamsabadi et al. (2007):

$$A = \frac{y_{\max}}{2K_{50}y_{\max} - P_{ult}} \text{ and } B = \frac{2\left(K_{50}y_{\max} - P_{ult}\right)}{P_{ult}\left(2K_{50}y_{\max} - P_{ult}\right)} \tag{2.8}$$

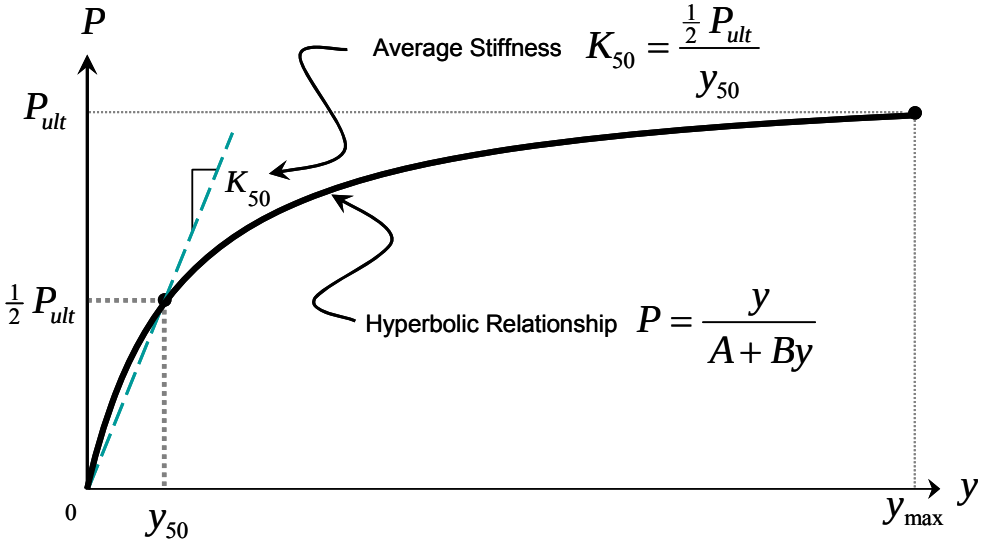

Figure 2.6. Hyperbolic load deflection relationship used by Shamsabadi et al. (2007)

Shamsabadi et al. (2007) developed an alternative, relatively simplified, hyperbolic model by fitting the *A* and *B* parameters in Eq. 2.6 to experimental test data. The parameters *A* and *B* were specifically determined for an abutment wall with a backfill height of 5.5 ft for both cohesive and cohesionless backfill soils and are given per linear ft of wall width. Their recommended values were A = 0.022 in/kip/ft and 0.011 in/kip/ft for cohesive and granular backfill, respectively, and B = 0.0297 1/kip/ft for both granular and cohesive backfill. This model is referred to by Shamsabadi et al. (2007) as the Hyperbolic Force-Displacement (HFD) model.

Shamsabadi et al. (2007) extended the capacity prediction model of Shamsabadi et al. (2005) to evaluate load-deflection behavior. In this model, a hyperbolic model is used to describe the behavior of backfill soils as characterized from triaxial tests. This hyperbolic model allows strains to be calculated in "slices" through the passive wedge as a function of the stress level in that wedge. Stress level is defined as the ratio of the mobilized shear stress to the ultimate shear strength. Through this process, for given lateral load, the summation of the interslice force differentials yields the mobilized horizontal passive capacity F_{ih}, while the displacement of the entire logarithmic-spiral failure surface at the location of the wall can be calculated by summing the displacements Δy_{ij} of all slices (Figure 2.6). The result is hyperbolic in shape, but is not described by simple equations such as Eq. 2.6 and instead is determined through a computer program such as a spreadsheet. This model is referred to by Shamsabadi et al. (2007) as the logarithmic-spiral failure surface combined with hyperbolic stress-strain relationship (LSH) model.

Finite Element and Finite Difference Modeling

Many studies have investigated the capacity and load-deflection relationships for walls under passive conditions using finite element and finite difference methods. Duncan and Mokwa (2001) review the results of many of those studies, and report that they have generally found the log-spiral surface to accurately reflect the computed failure surface from the models. Moreover, they found that log-spiral solutions for passive capacity are much more compatible with results of element modeling than the Coulomb model.

Shamsabadi and Nordal (2006) used 3D finite element modeling to simulate stiffness degradation behavior of the abutment-backfill systems, which has been observed during major seismic events (Goel and Chopra, 1995). Simulations of the present experimental setup using 2D and 3D finite element modeling was conducted by Shamsabadi (2006, personal communication) using the computer program Plaxis. The Plaxis 2D and 3D results were nearly the same and were in good agreement with the experimental data. The similarity of the 2D and 3D results supports the notion that nearly plain-strain conditions were likely to have been achieved during testing.

Simplified Design Criteria

To simplify the process of developing load-deflection curves for use in routine bridge design, the Caltrans Seismic Design Criteria (2006) adopts a bi-linear model as shown in Figure 2.7. The model is described by two parameters: initial stiffness (K_1) and passive capacity (P_{ult}). Passive capacity P_{ult} is not based on fundamental theory (Section 2.1), but rather on the result of a field test performed at UC Davis involving clay backfill (Romstad et al., 1995). As shown in Figure 2.7, the slope parameter K_1 is determined using a secant modulus through the origin and a point on the experimentally based load-deflection curve corresponding to 1 inch lateral displacement (i.e., K_1 is not the same as K_{50} in Figure 2.6). This results in a stiffness of approximately 20 K/in/ft for the cohesive backfill. Based on this test, P_{ult} is calculated using a uniform pressure of 5.0 ksf acting normal to the wall. The overall abutment stiffness is calculated in SDC (2006) as

$$K_{abut} = 20\frac{kip/in}{ft} * w * \frac{H}{5.5\,ft} \tag{2.9}$$

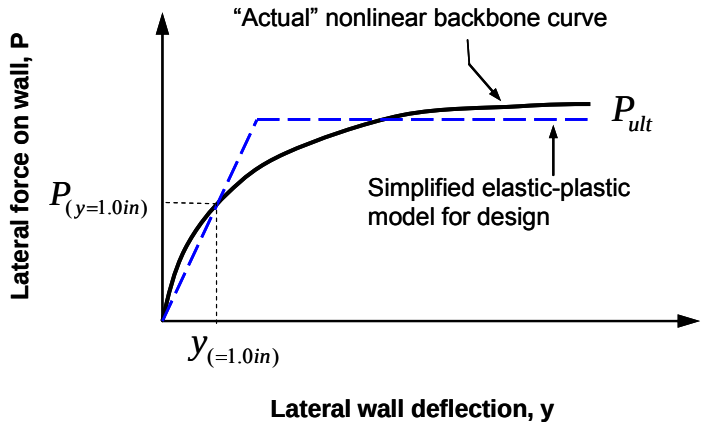

Figure 2.7. Elastic-perfectly plastic model used in Caltrans Seismic Design Criteria (2004) for load deflection behavior of abutment backwalls

If the approach shown in Fig. 2.6 were applied to the UCD test results, the average abutment stiffness based on 50% of P_{ult} would be K_{50} = 25 K/in/ft (Shamsabadi et al. 2007). The overall abutment stiffness could then be calculated as:

$$K_{abut} = 25\frac{kip/in}{ft} * w * \frac{H}{5.5\,ft} \tag{2.10}$$

where H= height of the wall [ft] and w = width of the wall [ft].

Design guidelines for load-deflection relationships of walls have also been presented by US Navy (1982), later adopted by the Canadian Geotechnical Society (1992). The relationship is based on an experiment involving an 0.6 m tall wall that was displaced into a sand backfill (Tschebotarioff and Johnson, 1953). This and other similar relationships are reviewed below.

2.3 Large-Scale Tests of Abutment Systems

A number of tests have been performed at laboratory scale to investigate passive earth pressures against retaining structures (Tschebotarioff and Johnson, 1953; Schofield, 1961; Rowe and Peaker, 1965; Mackey and Kirk, 1968; Narain et al., 1969; James and Bransby, 1970; Roscoe, 1970; Carder et al., 1977; Fang et al., 1994; Gadre and Dobry, 1998). Many of these tests have been used to develop empirical relationships between passive pressure formation and normalized

wall displacement ($K_p/(K_p)_{max}$ vs $\Delta H/H$). Results from selected laboratory-scale experiments, and some field-scale experiments, are summarized in Figure 2.8. In the following we focus on full-scale tests, which are desirable because the stresses acting in the soil replicate those in real specimens. This is especially important given the granular nature of typical wall backfills.

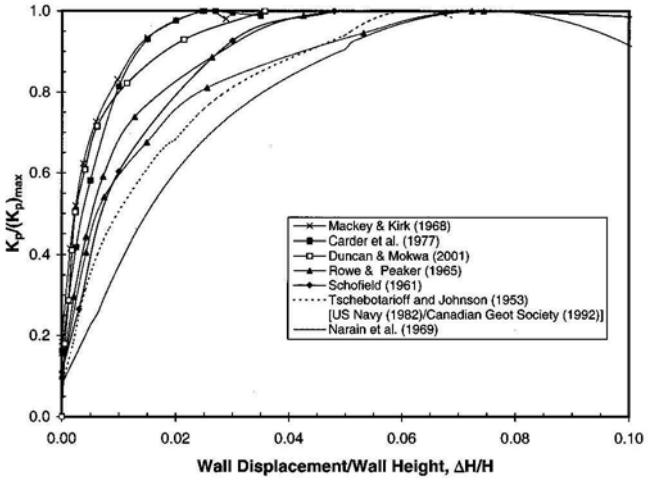

Figure 2.8. Curves showing development of normalized passive resistance as function of normalized wall displacement based on tests by various investigators (Rollins and Sparks, 2002)

One of the first large-scale tests of passive earth pressures was the aforementioned cyclic tests of abutments by Romstad et al. (1995). Those tests involved a 10.0 ft (width) by 5.5 ft (height) wall specimen that was displaced both into the backfill (simulating longitudinal deck excitation) and along the backfill (simulating transverse excitation). The actuators pushing against the abutment walls reacted against a pile cap. The failure surface was observed to plunge down into the backfill from the base of the wall and then rise towards the surface at increasing distance from the wall. The failure was 2D in geometry because of a rigid connection of concrete wingwalls to the backwall. The backfill consisted of cohesive compacted soil with S_u = 2.0 ksf. As mentioned above, those tests form the basis of current Caltrans seismic design criteria.

Duncan and Mokwa (2001) tested an anchor block of dimensions 6.2 ft (width) by 3.6 ft (height). The block was pushed first against natural soil consisting of hard sandy silt and sandy clay and a second time against compacted gravel backfill. The actuators pushing against the anchor block reacted against a pile group with a concrete cap. The failure zone in the soil was

not confined laterally, and hence was three dimensional (3D) in geometry. The test data were compared to predictions of the aforementioned Duncan-Mokwa hyperbolic model, which was implemented with a log-spiral (Terzaghi, 1943) estimate of passive capacity and a correction for the 3D geometry of the failure surface (Ovesen, 1964; Brinch Hansen, 1966). The comparisons of the analytical model to test data were favorable.

Rollins and Sparks (2002) tested a pile cap of dimensions 9 ft square by 4 ft deep. The cap was supported by a 9 pile group driven in a 3x3 configuration, and the cap was backfilled with compacted gravel only in the direction of push (i.e., there was no gravel on the sides of the cap). The pile cap was pushed laterally by two actuators reacting against a sheet pile reaction wall. Rotation of the cap was restrained only by the underlying piles. For this experiment, resistance to translation was provided by base friction on the cap, pile-soil-pile interaction, and passive resistance of the backfill. Accordingly, an experimental load-deflection relationship solely for the passive resistance could not be developed. Analyses of each resisting mechanism were performed, and for the case of passive resistance the ultimate load was calculated using the log-spiral method and the load-deflection relationship was evaluated using normalized curve of $K_p/(K_p)_{max}$ vs $\Delta H/H$ based on prior experiments (Narain et al., 1969).

Rollins and Cole (2006) performed full scale testing of a pile group and cap with and without backfill. The pile cap was pushed horizontally with hydraulic jacks reacting against a pile group. Four different backfill soils were used, consisting of clean sand, silty sand, fine grained gravel, and course grained gravel. The tests without backfill were used to correct for the pile resistance at the base of the cap. During testing, the pile cap was loaded to prescribed displacement levels and than cycled several times. The unloading portion of the cyclic testing was sufficient to form gaps between the wall and soil. The soil wedge was not confined laterally and formed a 3D surface. The failure surface through the backfill was observed using polystyrene columns, which were offset by the shear and excavated following testing. The observed failure surfaces had log-spiral shapes. The shapes of the failure surface, the ultimate passive loads at failure, and load-deflection behavior were reported for all four backfills. Cole and Rollins (2006) went on to analyze the walls. After adjusting the applied loads for 3D effects (Brinch Hansen, 1966), the test results were compared to theoretical predictions. The capacities obtained during the tests agreed most favorably with predictions made using the log spiral method. Less favorable capacity predictions were obtained using Rankine earth pressure theory

(which underpredicted) and Coulomb theory (which overpredicted). The load-deflection data were consistent with predictions of the Duncan and Mokwa (2001) hyperbolic model. Less favorable predictions were obtained from the Caltrans Seismic Design Criteria and US Navy design guidelines. The Caltrans Seismic Design Criteria underestimated the soil resistance by about 40 to 70% for deflections less than 0.01H. The US Navy guidelines underestimated (by 30 to 50%) the loads required to achieve displacements less than 0.036H. The cyclic test data showed that the reloading stiffness decreases with increasing peak displacement levels.

Bozorgzadeh et al. (2006) tested a bridge abutment at the UCSD Englekirk Structural Engineering Center in La Jolla, CA. The wall specimen was constructed at 50% of prototype scale with dimensions of 15.5 ft (width) by 5.5 ft (height) and 1.5 ft (thick). Unlike the other specimens described above, the wall was constructed integrally with two wingwalls that laterally confined the specimen. Moreover, the backfill was sloped at 2H:1V from the base of the wall, which forced the failure surface to occur at the transition between the backfill and natural soil. The wall was pushed with five hydraulic actuators reacting against a movable reaction wall consisting of four concrete reaction blocks, which were post-tensioned to a deep pile foundation. The vertical motion of the wall was restrained during the tests. The backfill consisted of clayey sand and silty sand. Comparisons to theory were made, although some of the conditions assumed in the theoretical models were not present in this series of experiments.

3 EXPERIMENTAL SETUP

3.1 Loading System and Specimen Configuration

The specimen, located at the UCLA-Caltrans test site in Hawthorne, California, consists of a full-scale (in height) model of a backwall with dimensions of 8.5 ft (height) by 15 ft (width) by 3 ft (thick). The wall is located at a clear distance of 11 feet from a reaction block with dimensions of 24 ft in length, 12 ft in width and 6 ft in height. The reaction block provides a load capacity of 3000 kips in the linear range, which exceeds the applied forces to the test specimen by a factor of six. As shown in Figure 3.1, five hydraulic actuators were installed between the test specimen and the reaction block to control the horizontal and vertical displacement of the wall.

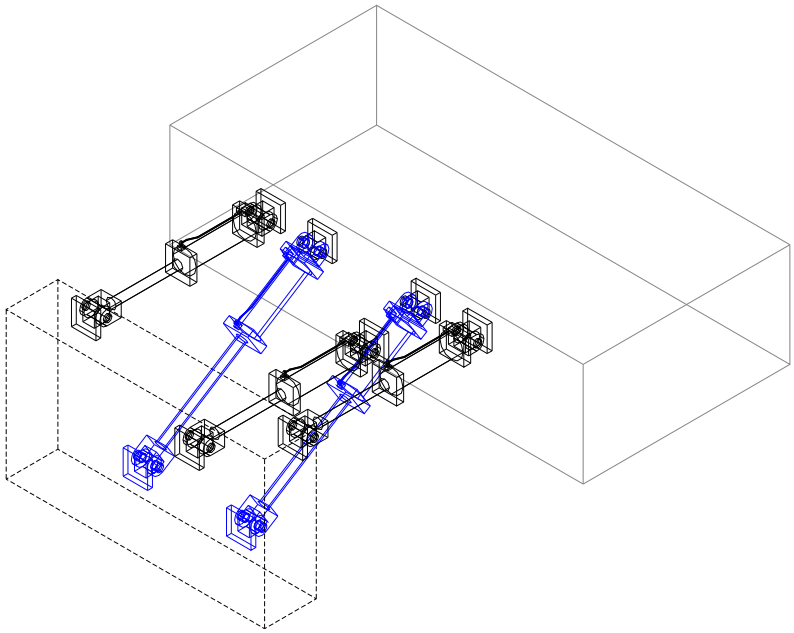

Figure 3.1. Actuator configuration

The natural clayey soils at the site were excavated as shown in Figure 3.2 so that the failure plane would be entirely within backfill. Side panels of plywood were erected to simulate wingwalls. These panels are located approximately 0.3 m from the backwall. To reduce the friction between the sidewalls and the backfill, the plywood wing walls were furnished with two layers of 0.006 in PVC foil.

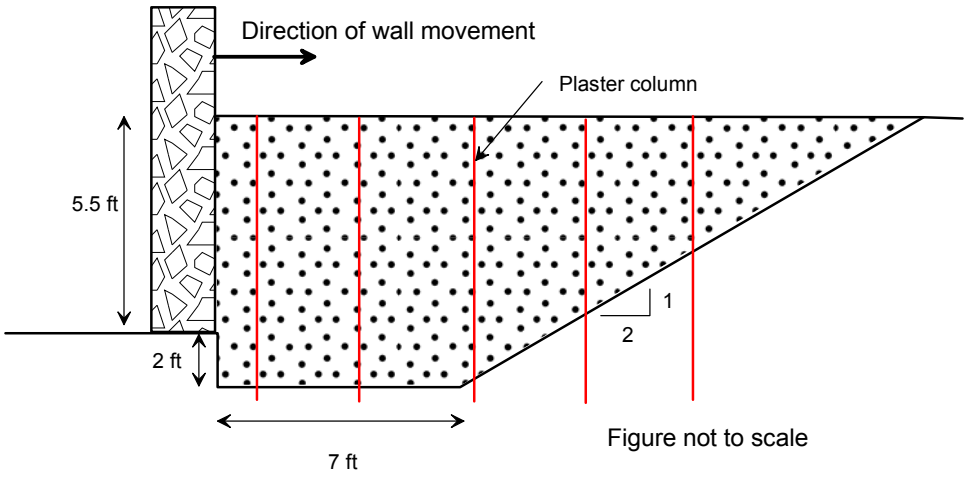

Figure 3.2. Schematic cross section through test specimen illustrating the shape of the excavated surface and backfill

Testing was conducted under displacement control, in which horizontal displacements (normal to the wall) were prescribed and all other displacements and all rotations were held to zero. Forces and displacements of all actuators were recorded individually using an MTS control system and the corresponding Flextest GT Software. Further details on the control system are provided in Section 3.3.

3.2 Sensor Layout

Five Transtek Linear Variable Differential Transducers (LVDTs) were installed to control the wall movement. As shown in Figure 3.3, three horizontal LVDTs were oriented parallel to the centerline of the three horizontal actuators. The average of these three displacements was used for control purposes. Figure 3.4 shows a hollow tube-section steel truss that was installed at a clear distance of 0.6 m (2 ft) above the top face of the wall to serve as a reference frame. Metal rods, attached to the frame and vertically extending over the height of the wall as shown in

Figure 3.5, were used to install the horizontal LVDTs at the centerline of each horizontal actuator. Two vertical LVDTs were directly attached to the frame and the wall, where they rested on a steel base plate to assure unrestricted horizontal movement (Figure 3.6). Those LVDTs were aligned with the diagonal actuators to enforce zero vertical wall movement. String potentiometers (SP) measured movements of the wall in the direction perpendicular to the push direction and also to movements of the reaction block parallel to the push direction.

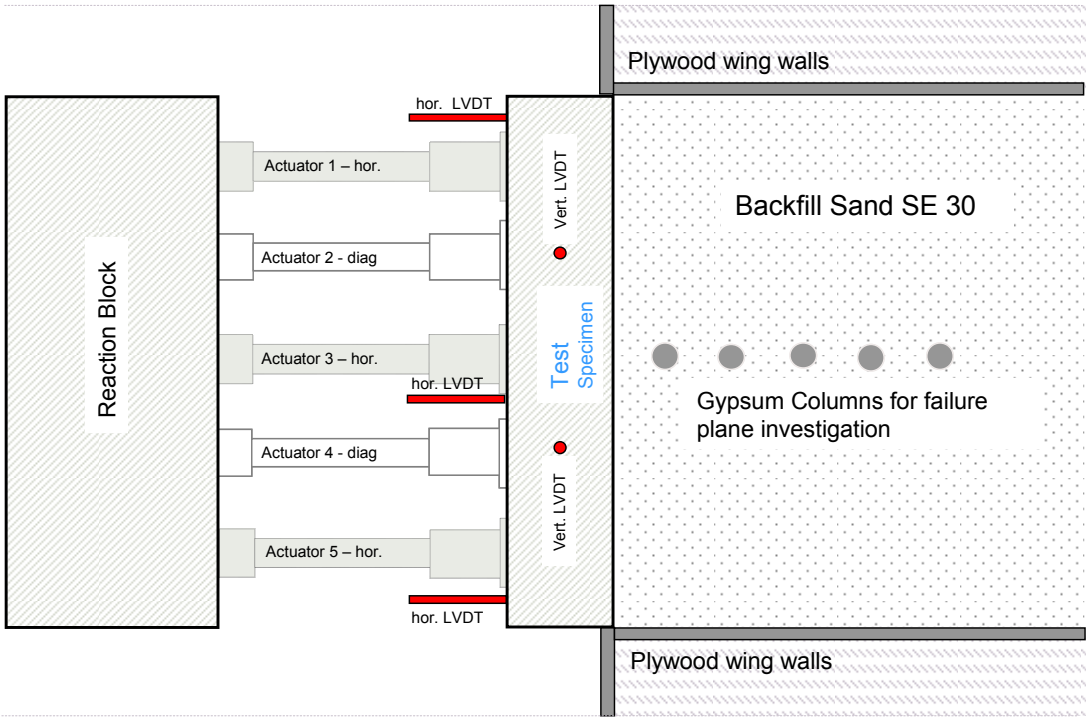

Figure 3.3. Plan view of test setup with instrumentation

Figure 3.4. Photograph of actuator configuration

Figure 3.5. Photograph of horizontal LVDT attached between a metal bar extension and the test specimen

Figure 3.6. Photograph of vertical LVDT at top face of the test specimen

3.3 Control System

A four-channel MTS Flextest GT Control System and a single-channel 407 controller were used to record and control the forces and displacements of the hydraulic actuators. Actuators 1, 2, 3 and 5 were connected to the MTS Flextest GT control system, while actuator 4 was driven by the single channel 407 controller. Forces and displacements of actuators 1, 2, 3, and 5 were connected to the adjacent input channels in the 4 channel controller (DC Slot 3-2 to 6-2 and AC Slot 3-1 to 6-1, respectively) while the forces and displacements of actuator 4 were read into the program as auxiliary inputs (Analog Input 1 and 2, Slot 3-3).

The displacements were measured with five LVDTs which consisted of four AC LVDTs (Alternate Current Linear Voltage Differential Transducer) and one DC LVDTs (Direct Current Linear Voltage Differential Transducer). The single DC LVDT was connected to the 407 controller. The parallel wall displacement and the motion of the reaction block were two more Auxiliary Inputs. (Analog Input 3 and 4, Slot 3-3).

The pretest data (movement without backfill soil) were recorded using Q330 data loggers. The data for the wall displacement with backfill soil were recorded directly using the Flextest Software of the Controller PC.

Further outputs were created using the "calculated output" option in which the control system internally calculates outputs through user defined equations. These additional outputs as well as there equations are shown below:

Table 3.1. Calculated Outputs from the MTS Flextest Controller

Calculated Output	Name	Equation	Description
1	Average Hz Disp Output	(Actuator 1 Hz Left Displacement + Actuator 3 Hz Center Displacement + Actuator 5 Hz Right Displacement) / 3	Describes the average horizontal displacement using the outputs of the 3 horizontal LVDT's
2	Total Horiz Act Force	(Actuator 1 Hz Left Force + Actuator 3 Hz Center Force + Actuator 5 Hz Right Force)	Sum of Forces in the 3 hor. Actuators
3	Total Vert Act Force	Actuator 2 Dg Left Force + Actuator 4 Dg Right Force)	Sum of forces of diagonal actuators
4	Total Net Horizontal Force	Total horiz Act Force + (Total Vertical act force *(9.5/sqrt(9.5^2+6^2)))	Pure hor. Force consisting of hor. forces from hor. actuators + hor. part from diag. actuator
5	Total Net Vertical Force	Total Vert Act Force *(6/sqrt(9.2^2 + 6^2)	Vertical part of diag actuator force

The displacement sensors were calibrated before the test and the calibration constants as well as the sensor polarities were inputted in the station setup of our control program. The polarity of the LVDT 1, 3 and 5 was inverted, meaning that the movement of the wall in positive x-direction implies extension of the LVDTs. The internal load cells of the actuators were calibrated in past tests and were adjusted to the load cell of actuator 1. A summary for all the calibrations and program inputs is given in the table below:

Table 3.2. Internal Calibration factors

channel	Actuator:		*1*	*2*	*3*	*4*	*5*
	HSM:		1	3	1	4	2
	Controller:		MTS Flextest	MTS Flextest	MTS Flextest	407	MTS Flextest
FORCE	sensor	Servovalve polarity	Invert	normal	normal		normal
		Full scale range	-200	-400	-400	200	-400
		Conditioner type	493.25 DC	495.25 DC	493.25 DC		493.25 DC
		calib. file	wall test 760.scf	wall test X050804A.scf	wall test X050809A.scf		wall test X050805A.scf
	calibration	Total Gain	611.5600	482.1600	480.7700	611.5600	481.0000
		Post amp	1.2741	1.0045	1.0016	---	1.0021
		Excitation	10.0000	10.0000	10.0000	10.0000	10.0000
		Delta K	0.9824	1.0000	1.0000	0.9824	1.0000
DISPL		LVDT polarity	invert	normal	normal		normal
		full scale	-5	-5	-5	5.475	-2 to 8
		File name	ac_lvdt_E	ac_lvdt_B	ac_lvdt_D		ac_lvdt_C
		total gain	4.4124	4.366	4.1964	1.0012 V/V	4.264
		post amp	1.1031	1.0915	1.0491		1.066
		Excitation	5V	5	5	10	5
		phase	90.2 deg	90.2 deg	90.2		90.2
		Delta K	1	1	1	1	1

The diagonal actuators (Figure 3.1) were used to restrain vertical motion of the abutment wall. For both controllers, this boundary condition can be enforced using the option "initial set point" in the control system. In this condition the initial readings are kept constant throughout the whole test while the diagonal actuators adjust their forces adjacently to satisfy the boundary condition. Figure 5.12-5.13 show the horizontal displacement versus the vertical displacement of actuators 2 and 4. When actuator 4 tripped at a displacement level of 1.0 inch it was adjusted manually to zero vertical displacement (initial setting).

The horizontal displacement was calculated using the average displacements of actuators 1, 3 and 5. The movement of the abutment wall was performed in two steps. A pretest up to a displacement level of 1.0 inch was conducted without soil backfill to estimate the frictional resistance of the wall provided by the natural underlying soil. The load was applied cyclically, only performing the positive displacement cycles. The load-displacement relationship is depicted in Figure 5.1.

After backfilling and compacting, the test was repeated and the wall was pushed against the backfill soil up to 7 inches. Forces were applied cyclically, but unloading was only performed up to a maximum negative displacement of 0.2 inches so as to always maintain positive contact stresses between backfill and wall (i.e., no gapping).

4 TEST SPECIMEN

4.1 Specimen Properties

The dimensions and geometry of the test specimen were described in Section 3.1. The wall was constructed from reinforced concrete. The concrete was normal weight with a specified unit weight of 145 pcf. Based on that unit weight and the wall dimensions, the weight of the wall specimen is estimated as 65.3 kips. Concrete cylinders taken during pouring were tested following the field testing. The stress-strain results are shown in Figure 4.1, and revealed an average strength of 5.8 ksi. Reinforcement steel with nominal yield capacity of f_y= 60 ksi was used. Figures 4.2-4.3 show the wall specimen before and after concrete pouring, with the former showing the steel configuration.

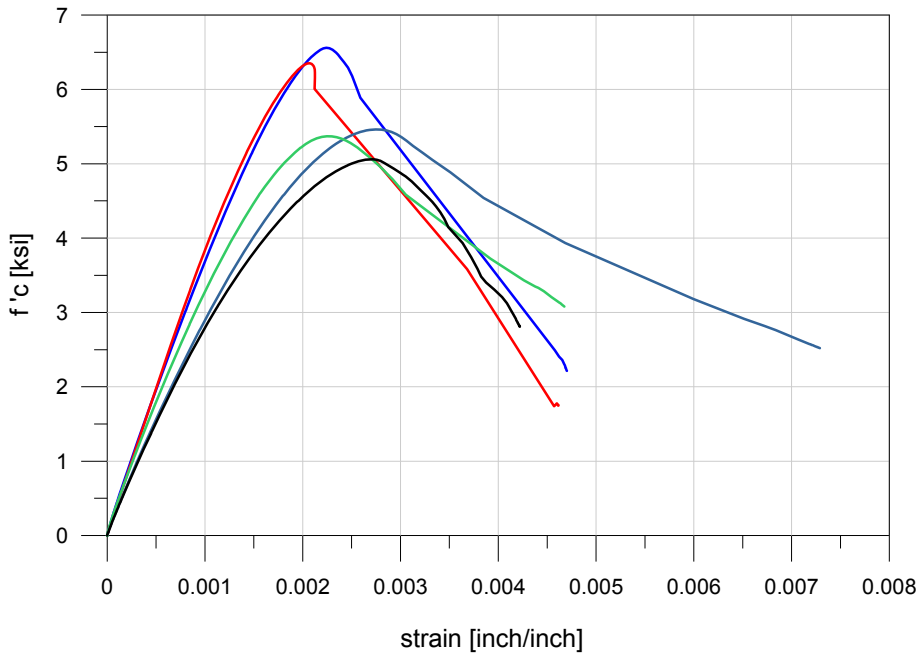

Figure 4.1. Results of unconfined compression tests on concrete cylinders

Figure 4.2. Reinforcement configuration in test specimen

Figure 4.3. Photograph of wall after concrete pour

4.2 Backfill Soil

The abutment wall was backfilled with a silty sand material known as sand-equivalent 30 (SE 30), which is a Caltrans standard material that is commonly found in bridge abutments (Earth Mechanics, 2005). The depth of the fill behind the wall varied with distance back from the wall as shown in Figure 3.2, although the nominal height above the base of the wall was 5.5 ft to be consistent with typical Caltrans practice. Gradation tests on the fill material (ASTM D1140) reveal the silty sand to be a well graded sand with silt (SW-SM) per the Unified Soil Classification System. The gradation curve is shown in Figure 4.4. The fines content is about 10% and D_{50} = 0.7-0.85 mm. The fines are silty and non plastic (unmeasureable plastic limit).

As shown in Figures 4.5-4.6, compaction curves were prepared for two bulk specimens of the backfill soil using modified AASHTO energy levels (ASTM D1557). The tests reveal an average maximum density of 127 pcf and an optimum moisture content of about 9%. All of the aforementioned testing was performed by Praad Geotechnical in Los Angeles, CA.

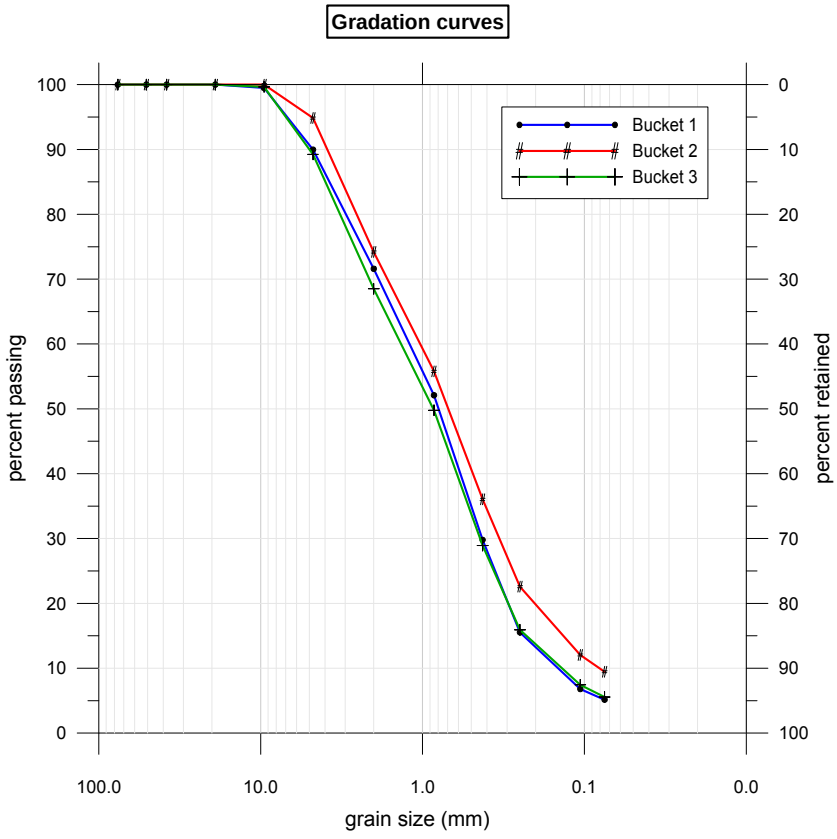

Figure 4.4. Gradation curves for three specimens of the silty sand backfill

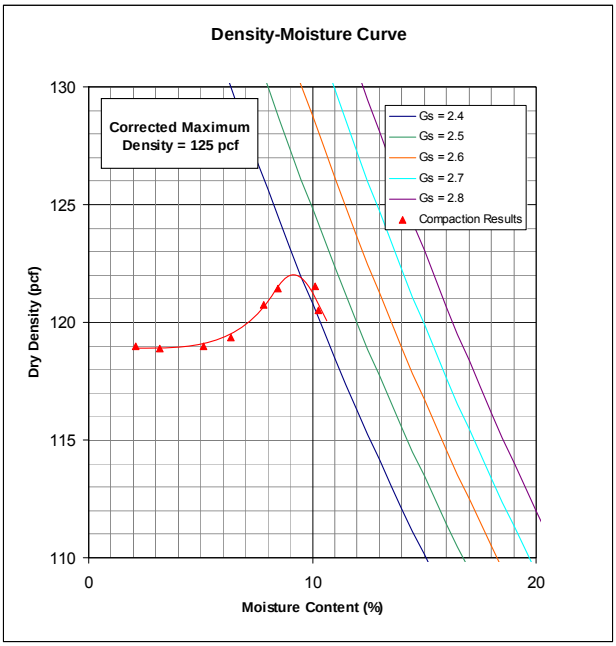

Figure 4.5. Compaction curve Bucket 1

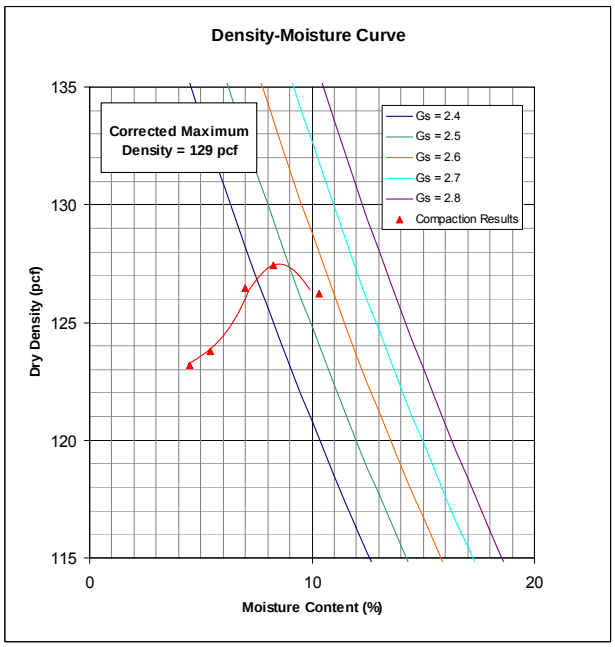

Figure 4.6. Compaction curve Bucket 2

The sand was placed in 1.0 ft lifts and compacted using vibratory compactors. Most of the backfill was compacted using the backhoe-mounted vibrator shown in Figure 4.7. Near the wall, a hand-operated vibratory compactor ("wacker") was used. Sand cone testing (ASTM D1556) performed during fill placement revealed that relative compaction levels (using the modified AASHTO standard) ranged from 94 – 111% (average = 99%). As-compacted water contents ranged from 4.7 to 9.3% (average = 6.6%), which is dry of optimum. The sand cone tests were performed at the locations shown in Figure 4.8. Figures 4.9-4.10 show the excavation of the test pad for sand cone testing and the sand cone device in place on the pad.

Figure 4.7. Vibratory compaction of backfill soils

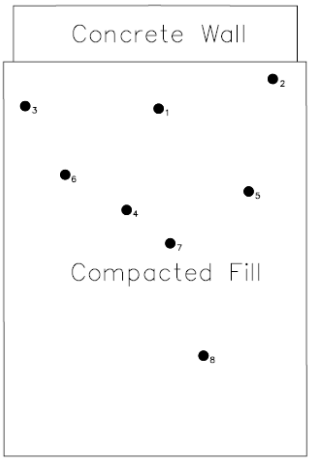

Figure 4.8. Sand cone testing locations

Figure 4.9. Excavation of pad for sand cone testing in compacted backfill

Figure 4.10. Sand cone installed on test pad

Triaxial compression tests (ASTM D2850) were performed on bulk samples that were compacted to a water content of approximately 6% and a relative compaction level of 96%. The testing was performed using UU protocols, but because the samples are unsaturated sands, effectively a consolidated drained (CD) condition is assumed. For a given specimen, the testing was performed by first placing the specimen under a prescribed cell pressure, then shearing the soil to failure by increasing the vertical (deviator stress). The cell pressure was then increased to two higher levels and the soil tested to failure at each level. Stress-strain curves resulting from the testing of two specimens subjected to the above load sequence are shown in Figure 4.11. Corresponding Mohr circles and linear failure envelopes for those specimens are shown in Figure 4.12. The failure envelopes in Figure 4.12 reveal a friction angle (ϕ) of about 40 degrees and a cohesion intercept of about 0.3-0.5 ksf. Axial strains at 50% of the failure stress ranged from 0.5-0.6%, which are slightly larger than the presumptive values of 0.3-0.5% given by Shamsabadi et al. (2007).

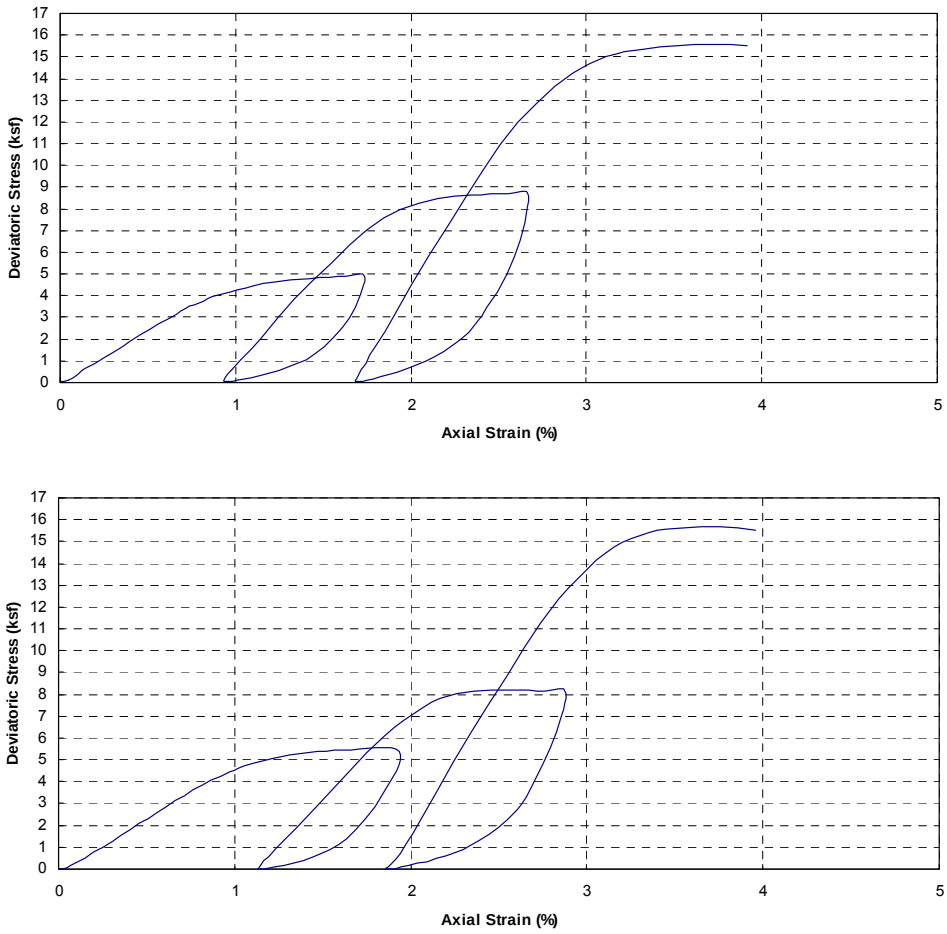

Figure 4.11. Stress strain curves from three cycles of triaxial compression tests on two different backfill specimens

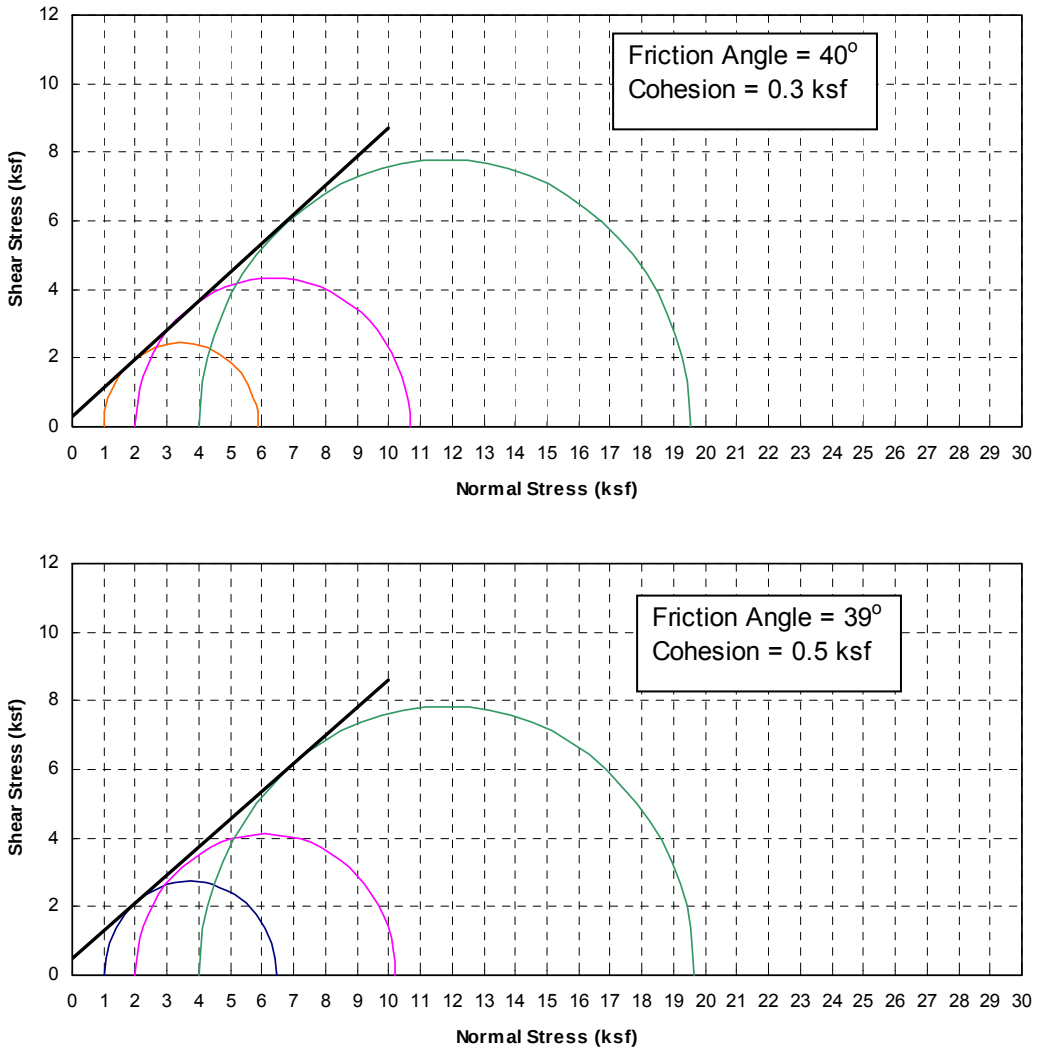

Figure 4.12. Mohr circles and Mohr-Coulomb failure envelopes at failure from triaxial compression tests on two different backfill specimens

5 TEST RESULTS

5.1 Load-Displacement Data

In this chapter we document the data collected during testing. The first test sequence involved displacing the wall with no backfill to establish the load-deflection relationship associated with base friction. The second sequence involved testing with backfill.

Figure 5.1 presents the load-deflection data collected without backfill. Five "cycles" of testing were performed in the positive direction only (towards the backfill), with the largest amplitude being 1.0 in (25 mm). The sudden jumps in the graph indicate that the internal displacement limits were reached. Those limits are set in the control system for safety reasons. The limits were extended and the test resumed, after it was assured that the specimen and the surrounding soil were in a stable condition. This process has no influence on the measured test data.

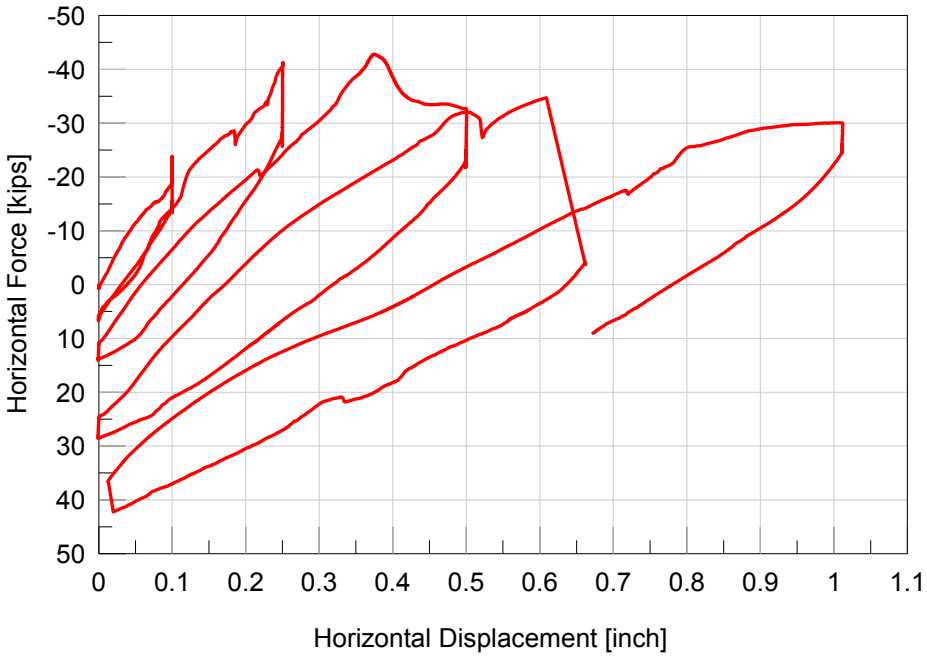

Figure 5.1. Load-displacement curve without backfill soil

Testing with the backfill in place was again performed with only positive cycles (displacements into the backfill). Unloading was carefully controlled so as to always maintain positive contact between the backfill and wall (no gapping allowed). Table 5.1 shows the loading and unloading sequence for the load displacement curve with backfill soil. The complete load-displacement response is plotted in Figure 5.2. As shown in Figure 5.2, the maximum lateral load for the test with backfill was about 520 kips, which was reached at a displacement of about 2.0 in.

Table 5.1. Loading and unloading sequence

initial ave reading at controller PC	Δ *displacement*	*start point [inch]*	*end point [inch]*	*total time of movement [sec]*
0.81				
0.91	0.1	0	0.1	60
0.88	-0.03	0.1	0.07	60
1.01	0.13	0.07	0.2	60
0.96	-0.05	0.2	0.15	60
1.21	0.25	0.15	0.4	60
1.11	-0.1	0.4	0.3	60
1.56	0.45	0.3	0.75	120
1.41	-0.15	0.75	0.6	60
1.81	0.4	0.6	1	120
2.31	0.5	1	1.5	120
2.16	-0.15	1.5	1.35	60
2.81	0.65	1.35	2	180
2.66	-0.15	2	1.85	60
3.81	1.15	1.85	3	360
3.66	-0.15	3	2.85	60
5.81	2.15	2.85	5	720
5.66	-0.15	5	4.85	60
7.81	2.15	4.85	7	720
6.81	-1	7	6	240

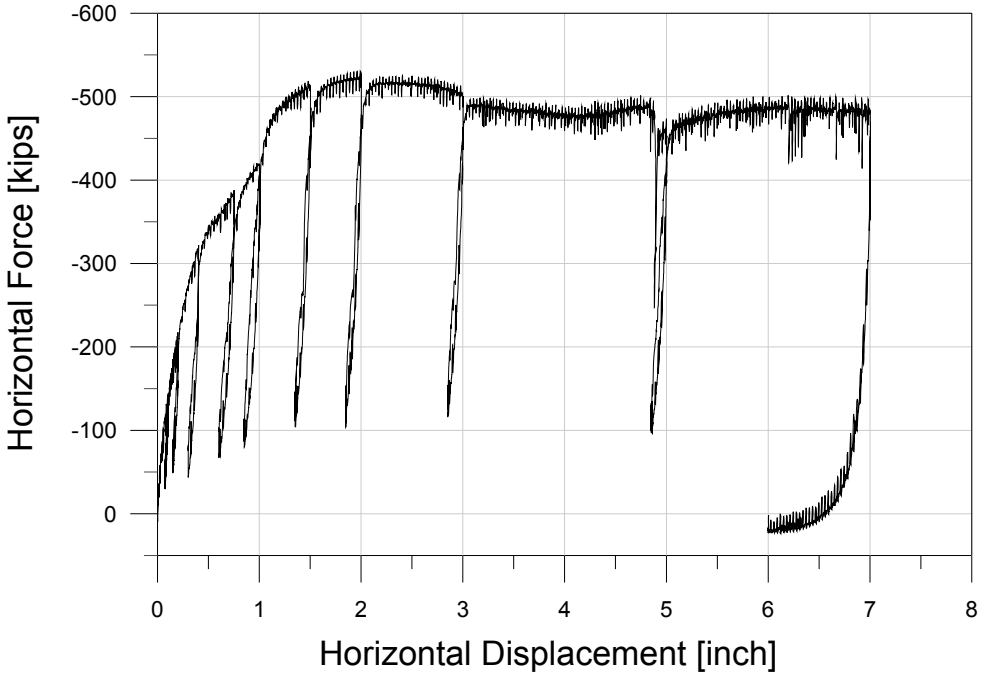

Figure 5.2. Load-displacement curve with backfill soil

The contribution of the wall base friction to the overall measured horizontal loads can be estimated by comparing the wall displacements with and without backfill soil. Figure 5.3 presents the hysteretic test data for both cases up to a peak displacement of 1.0 inch. Backbone curves were created using the peak load-displacement data associated with each initial cycle from both data sequences, with the results shown in Figure 5.4. Also shown in Figure 5.4 is the percent contribution of the base friction on the measured peak loads from the tests with backfill. The lateral resistance for the test without backfill reached a peak load of 40 kips at a lateral displacement level of 0.4 inches. The lateral resistance for a displacement of 1.0 inches dropped to about 30 kips. Based on the shear strengths of the natural clayey soils underlying the wall, the expected base resistance would be approximately 34 and 39 kips, which is consistent with the test data. For larger displacement levels (> 1.0 in.) the friction along the bottom of the wall was assumed to remain at 30 kips.

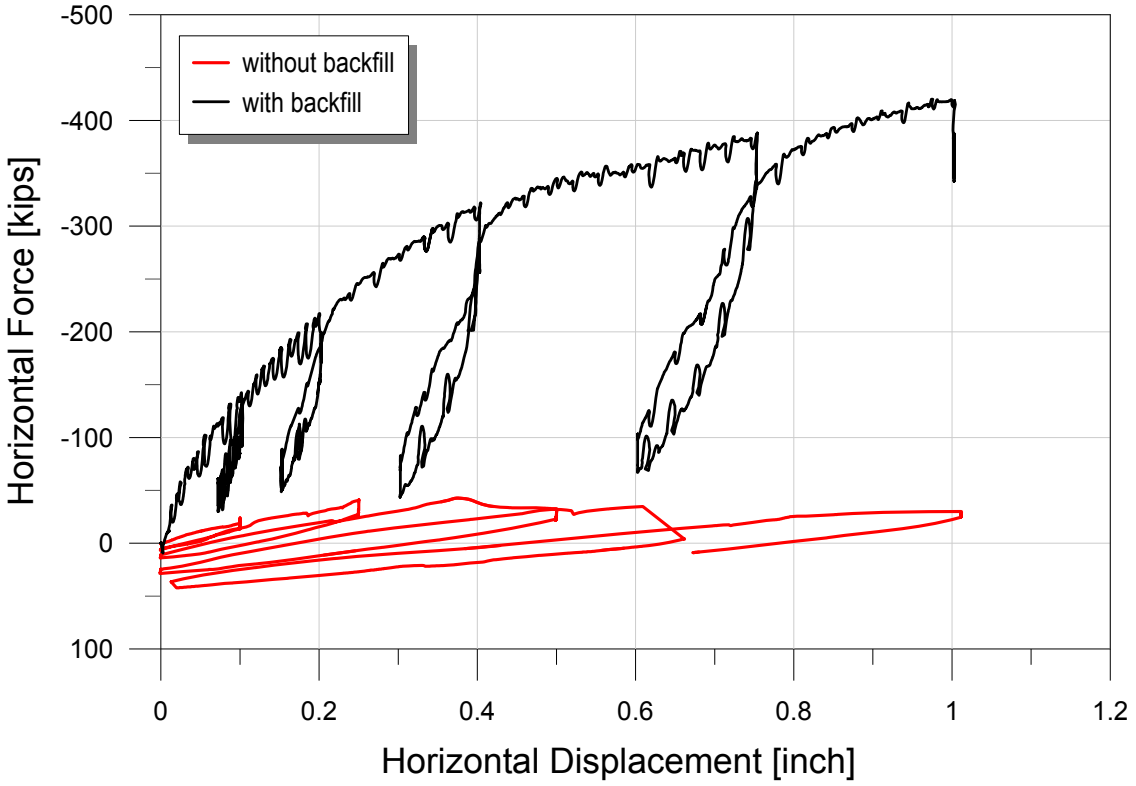

Figure 5.3. Load-deflection curves up to max displacement of 1.0 in with and without backfill

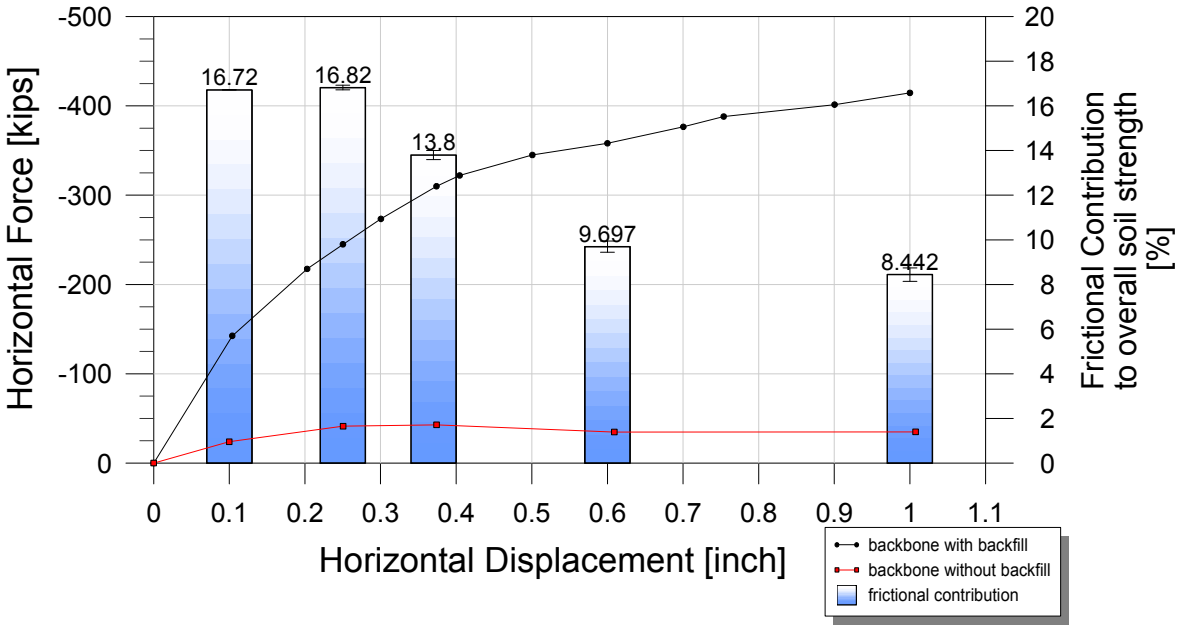

Figure 5.4. Backbone curves and contribution of base friction up to 1.0 inch displacement

5.2 Engineering Interpretations of Test Data

There are four principal interpretations of the test results that are of interest. The first is the ultimate passive capacity of the backfill, after correction for base friction effects. The second is the shape of the load-deflection curve prior to failure. The third is the interface friction angle (δ_{iw}) mobilized at the wall-soil interface. The fourth is the unload-reload moduli at different displacement levels.

The first two issues are addressed with the corrected load-deflection relationship shown in Figure 5.5. Three modifications were made to the results from Section 5.1 to prepare Figure 5.5. First, the base friction effects were removed so that the load-deflection data represents the backfill material response only. Specifically, the forces in Figure 5.2 were reduced by the base friction resultant shown in Figure 5.1. For displacements larger than 2 inches, the base friction resultant is taken as constant at 30 kips. Second, the data was smoothed by filtering and re-sampling at a lower sampling frequency. Third, the backbone curve has been smoothed over an irregularity associated with a temporary loss of vertical control between displacement levels of 0.5-1.0 inch.

As shown in Figure 5.5, the peak horizontal component of the passive force resultant was 490 kips, reached at a displacement level of 2.0 in. At this displacement level, the vertical component of the passive resultant was measured to be 125 kips. The vector sum of these two components provides the passive force capacity P_p = 506 kips. Assuming a triangular soil pressure distribution, the passive earth pressure coefficient would be

$$K_p = \frac{2P_p}{\gamma H^2 w} = 17.6 \tag{5.1}$$

If a uniform pressure distribution is used to represent the soil response, the ultimate horizontal earth pressure attained during the test was 490 kips/(15*5.5ft) = 5.94 ksf. If a triangular distribution is assumed, the base pressure would be 127pcf*5.5ft*17.6 = 12.3 ksf.

The passive force resultant drops for displacements larger than 2.0 in, which is expected given the dilatency of the backfill soil. For displacements larger than 3.0 inch, the horizontal component of the resultant force drops to approximately 450 kips. The corresponding passive pressure coefficient is K_p = 15.6 and the equivalent uniform pressure is 5.5 ksf.

The peak passive resistance occurred at a displacement of about 2.0 in, which corresponds to a normalized deflection $\Delta_{max}/H=0.03$. This result is in good agreement with normalized deflections of 0.03-0.052 measured by Rollins and Cole (2006).

An effective stiffness of the backbone curve can be evaluated as illustrated previously in Figure 2.6 in which a secant stiffness is taken through the origin and a point on the backbone curve at 50% of the ultimate load. This procedure is illustrated with the corrected test data in Figure 5.5, and results in an effective modulus of K_{50} = 247.5 / (0.33 inch*15ft) = 50.0 kips/inch/ft. The initial modulus of the backbone curve is shown by the blue line in Figure 5.5, and is K_i = 85 kips/in/ft.

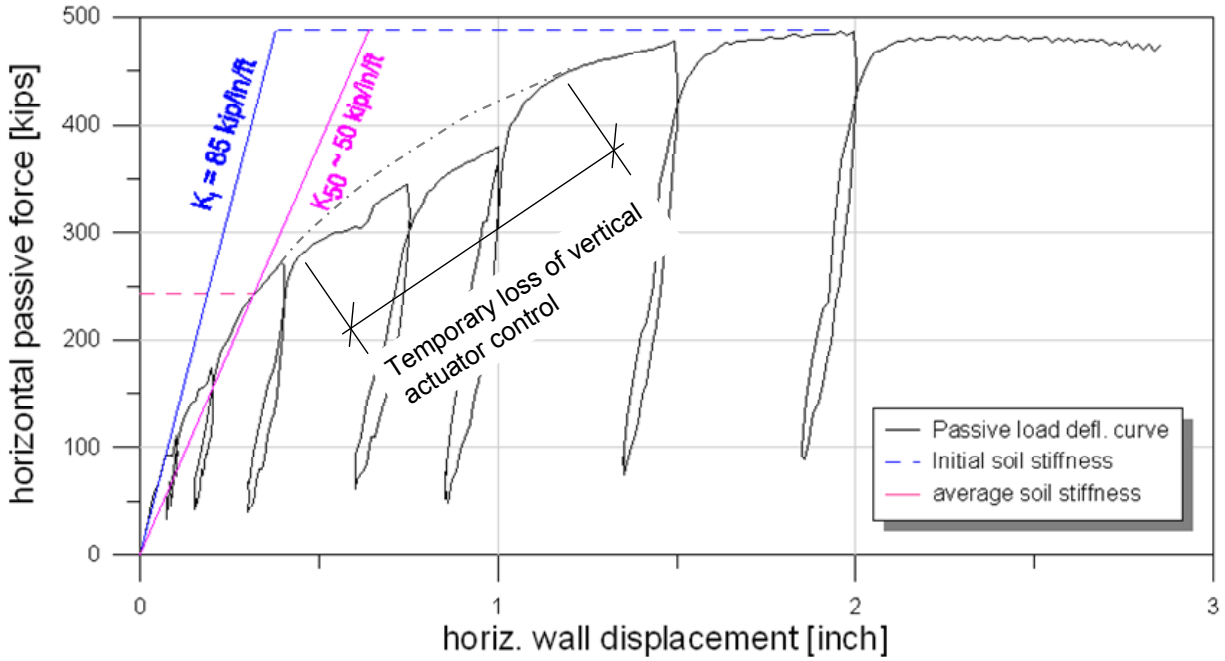

Figure 5.5. Load-deflection curves with initial and average stiffness of the backfill soil marked

The configuration of the hydraulic actuators provides the opportunity to resolve the horizontal and vertical components of the passive resultant force (third issue above). The data can be used to calculate the mobilized friction angle at the wall-soil interface (δ_{iw}). Figure 5.6 shows the measured horizontal and vertical components of the resultant force along with the vector sum (denoted as total force). The arctangent of P_v/P_h ratio, which is δ_{iw}, is plotted in Figure 5.7 (without unload-reload cycles for clarity). The mobilized friction angle varied with displacement level, with typical values being between 13 to 20 degrees. At the displacement

corresponding to the peak passive force (2.0 inch), the mobilized friction angle was δ_{iw}= 14.2 degrees, which is 0.36ϕ' (approximately 1/3ϕ'). At displacements corresponding to residual conditions (> 3.0 in), the mobilized friction angles range from approximately 13 to 20 degrees. Those mobilized friction angles may not correspond to the maximum possible interface friction at the wall-soil interface (i.e., shear failure did not necessarily occur). It is also noted that the wall face is relatively smooth (formed reinforced concrete), which may account for these relatively low mobilized friction angles.

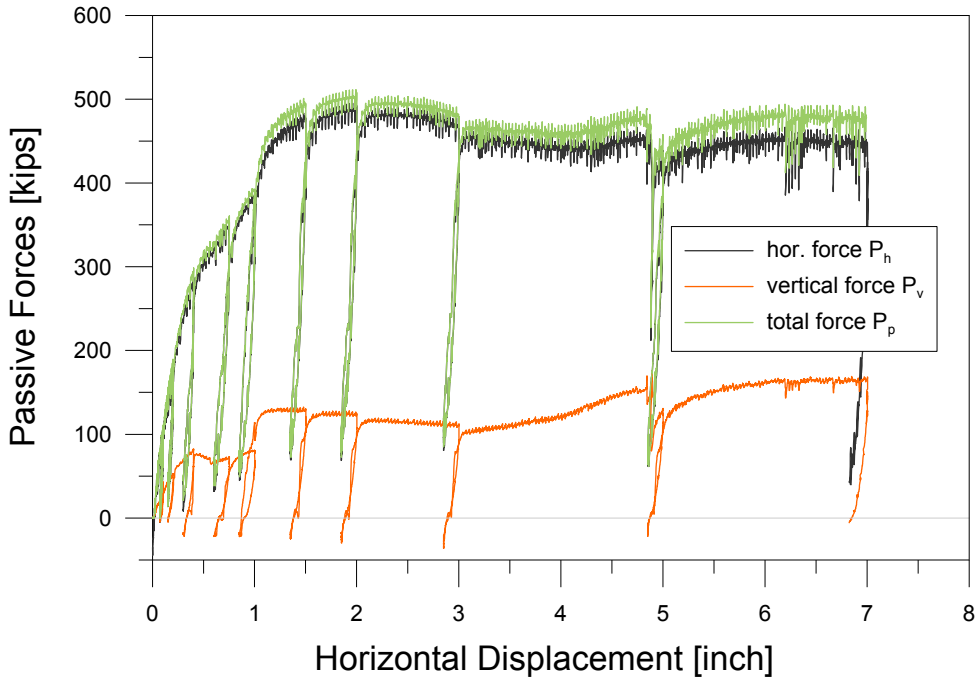

Figure 5.6. Comparison of the components of the passive earth pressure resultant force

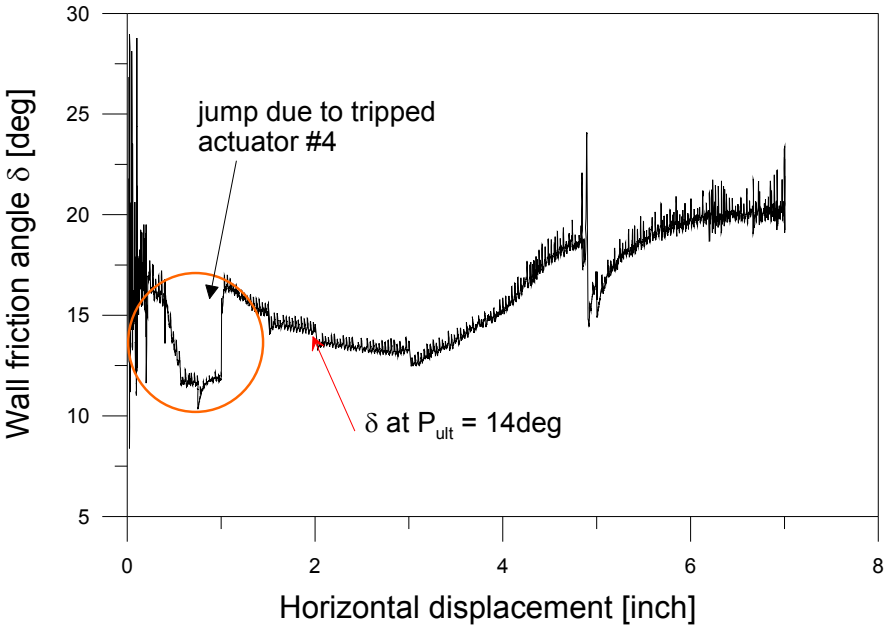

Figure 5.7. Friction angle δ versus horizontal displacement

The unload-reload cycles of testing provide the opportunity to evaluate unload-reload moduli (K_r) at various displacement levels (fourth issue above). The stiffness K_r was determined as shown by the red lines in Figure 5.8 by taking a secant modulus between points at the end of the unload-reload cycle and the cross-over point (just below the backbone curve). Moduli values computed in this way are summarized in Figure 5.9. The initial stiffness K_i (calculated above) is lower than any of the K_r values. K_r values reach a peak at a displacement level of 0.0625 inches and then degrade to a relatively stable value (insensitive to displacement level) of 2000-2200 kips/ft (130-145 kip/in/ft).

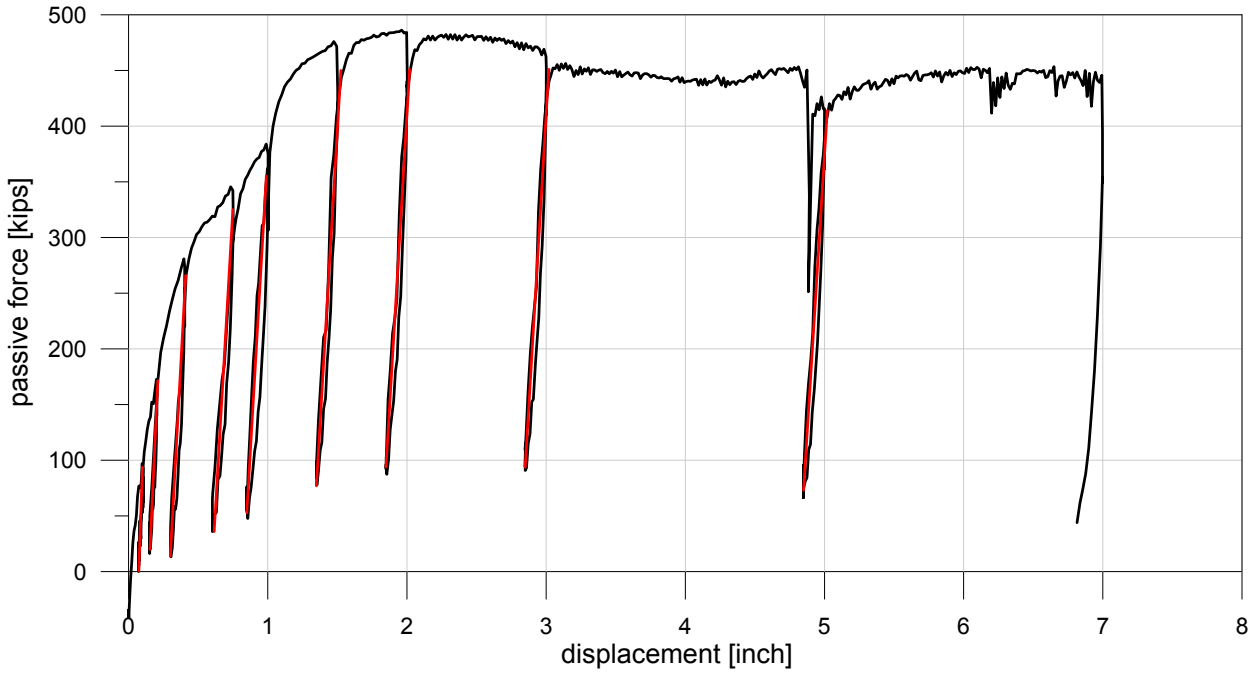

Figure 5.8. Load deflection curve with reloading stiffness indicated by red sloped lines

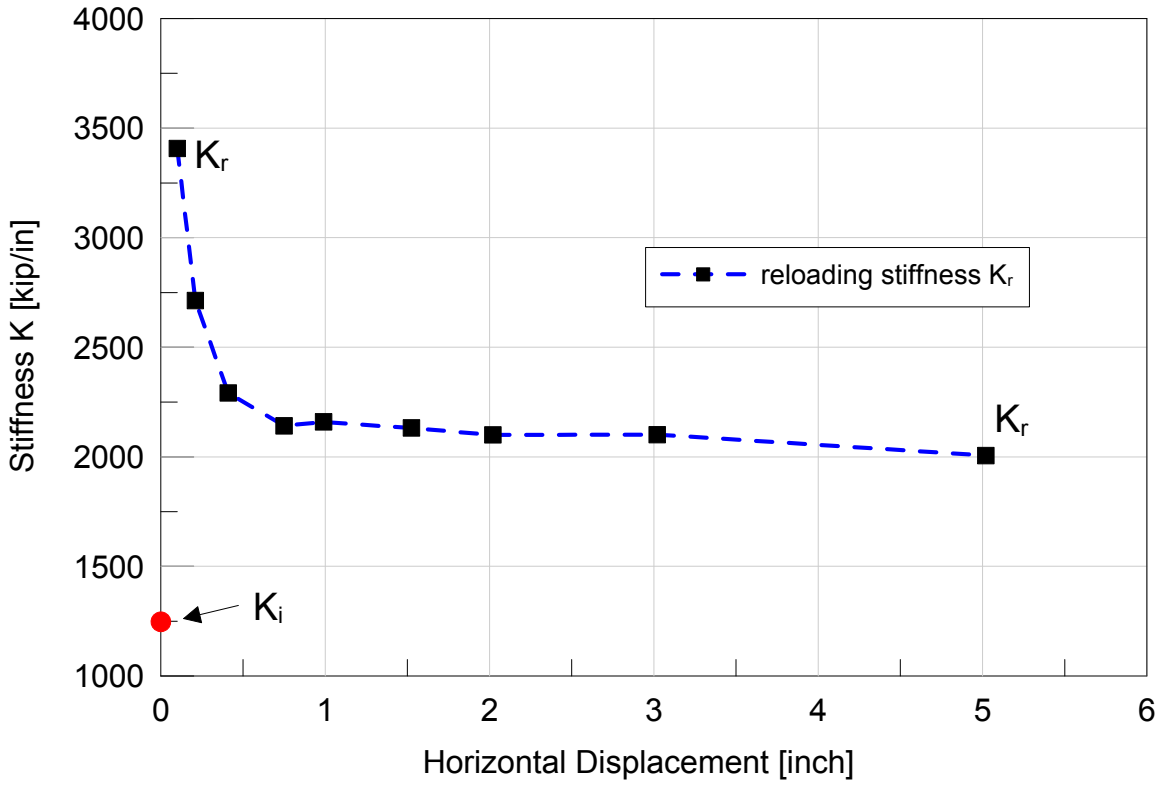

Figure 5.9. Reloading stiffness for each displacement level versus horizontal displacement

5.3 Ancillary Test Results

Data collected during the wall testing program provides the opportunity to evaluate the degree to which the desired boundary conditions were maintained (i.e., to check wall displacements perpendicular to the push direction horizontally and vertically) and to investigate the load-deflection response of the reaction block.

Horizontal wall movement perpendicular to the push direction is evaluated using a string pot in which one end is installed on the wall face and the other on the reference steel frame as its reference point (it should be noted that this horizontal movement was not considered in the control algorithm). This configuration of the string pot is depicted in Figure 5.10. Note that the change of length measured by this string pot is not directly horizontal movement perpendicular to the push direction (true displacements in this perpendicular direction are referred to subsequently as *normal wall displacement*). Neglecting wall rotation and flexure, normal wall movement (Δx) can be computed from the change of length of the string pot (i.e., D_0-D_M). and the measured displacement in the direction of loading (Δy) as follows:

$$\Delta x = 180'' - \sqrt{D_M{}^2 - (17 + \Delta y)^2} \tag{5.2}$$

where all dimensions are in inches. In Figure 5.10, D_{Noop} is the string pot reading that would correspond to no out-of-plane movement (Δx = 0). Figure 5.11 shows the measured string extension (black line), the theoretical string extension if Δx=0 (i.e., D_{Noop}), and the calculated displacement per Eq. 5.2. The permutation between 0.5 and 1.0 in of wall movement was due to a temporary loss of vertical control (discussed further below). The normal wall displacement is generally about 2% of the horizontal wall displacement. Some of this movement could be caused by small actuator misalignments creating eccentricities in loading, as well as nonlinearities in the sensor calibrations.

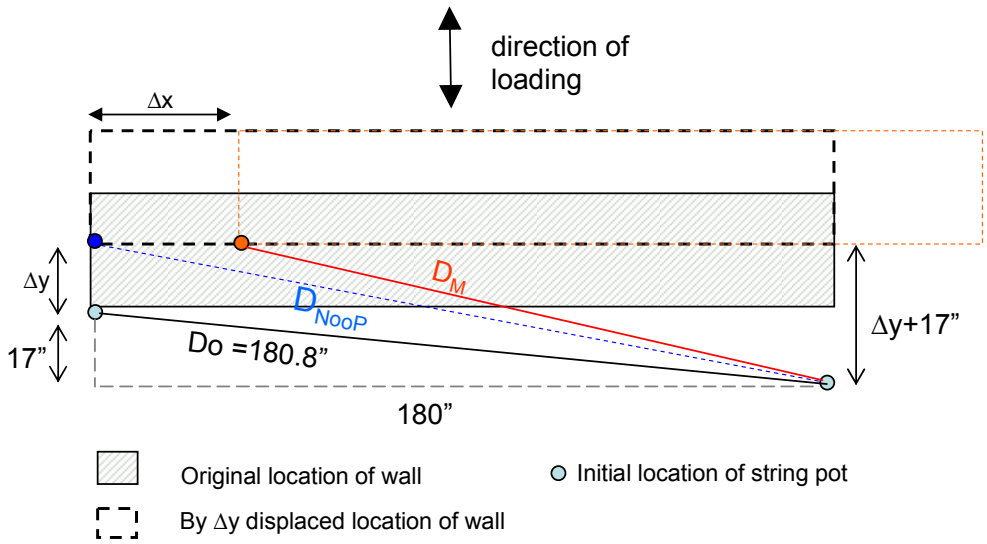

Figure 5.10. Schematic plan view of string pot setup and rigid body wall translation in two horizontal directions [Figure not to scale]

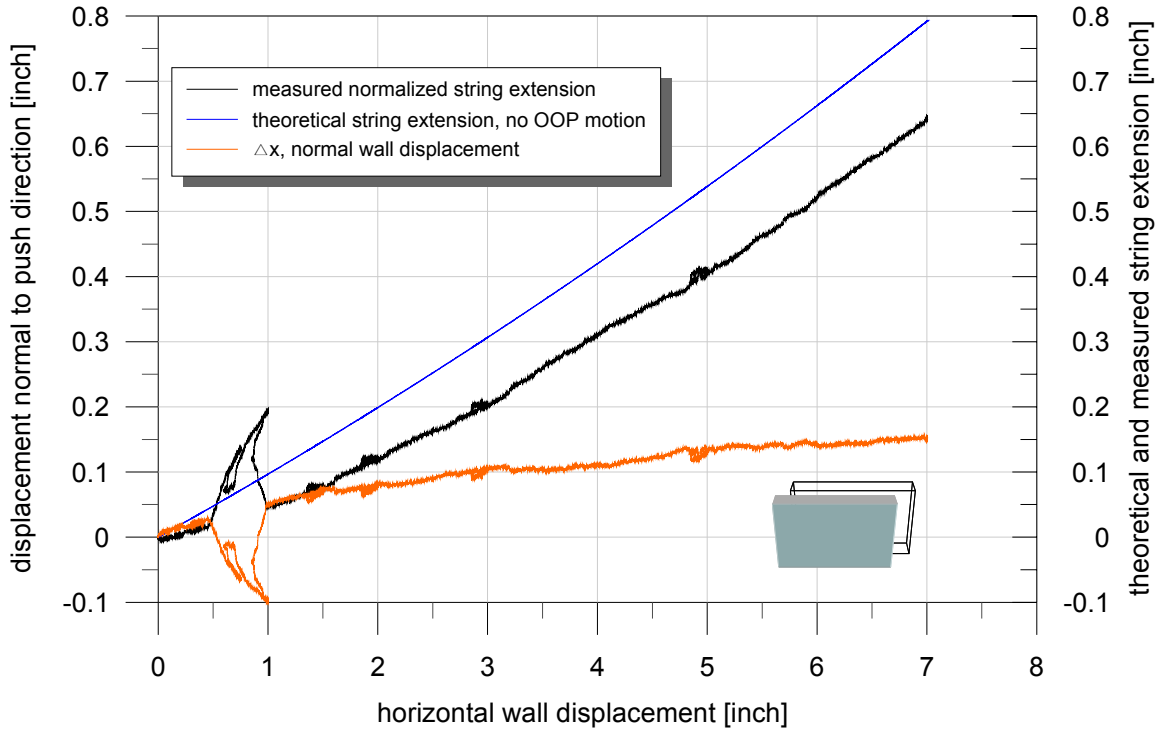

Figure 5.11. Displacement of the wall normal to the direction of push

Vertical wall movement was directly monitored by the control algorithm, with the intent of keeping this movement null. Figures 5.12 and 5.13 show the vertical displacement of Actuators 2 and 4 (diagonal Actuators) versus the horizontal displacement of the wall. It can be seen that the desired boundary condition of no uplift was successfully enforced throughout the test in Actuator 2. In Actuator 4, some upward movement occurred between horizontal displacements of 0.5 and 1.0 inch due to a temporary malfunction of a control system component. This was recognized during testing, and the zero displacement boundary condition was restored for the remainder of the test.

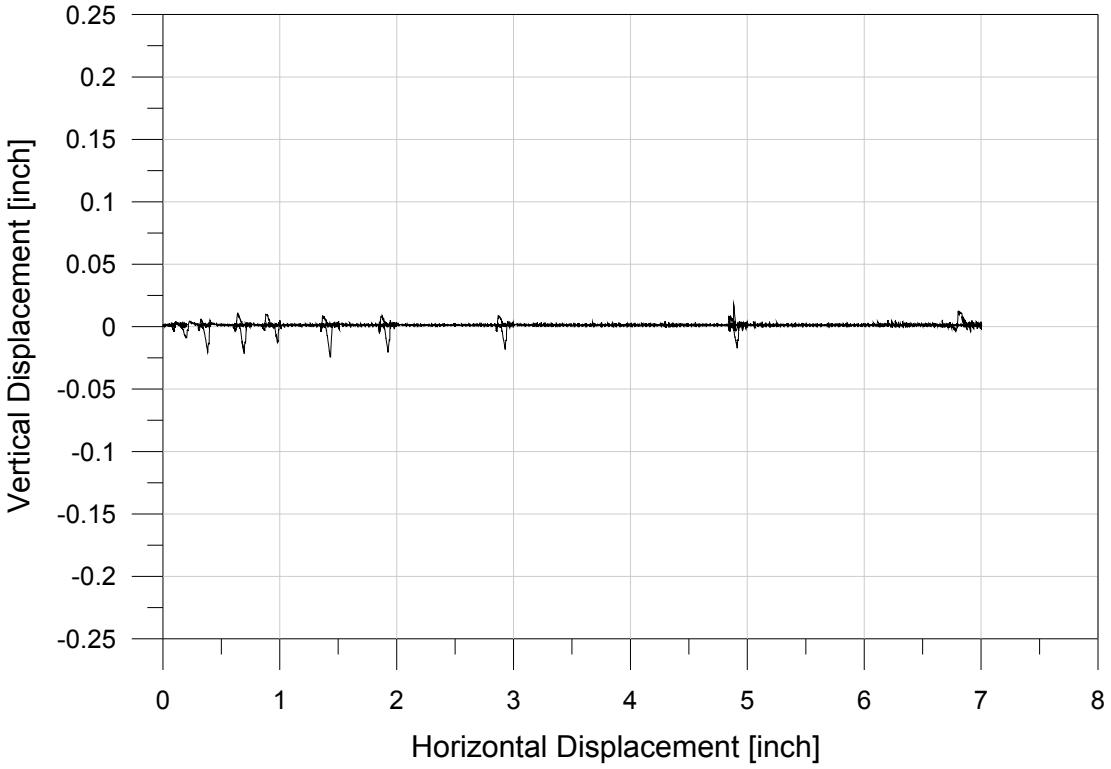

Figure 5.12. Vertical displacement (act 2) versus horizontal wall movement

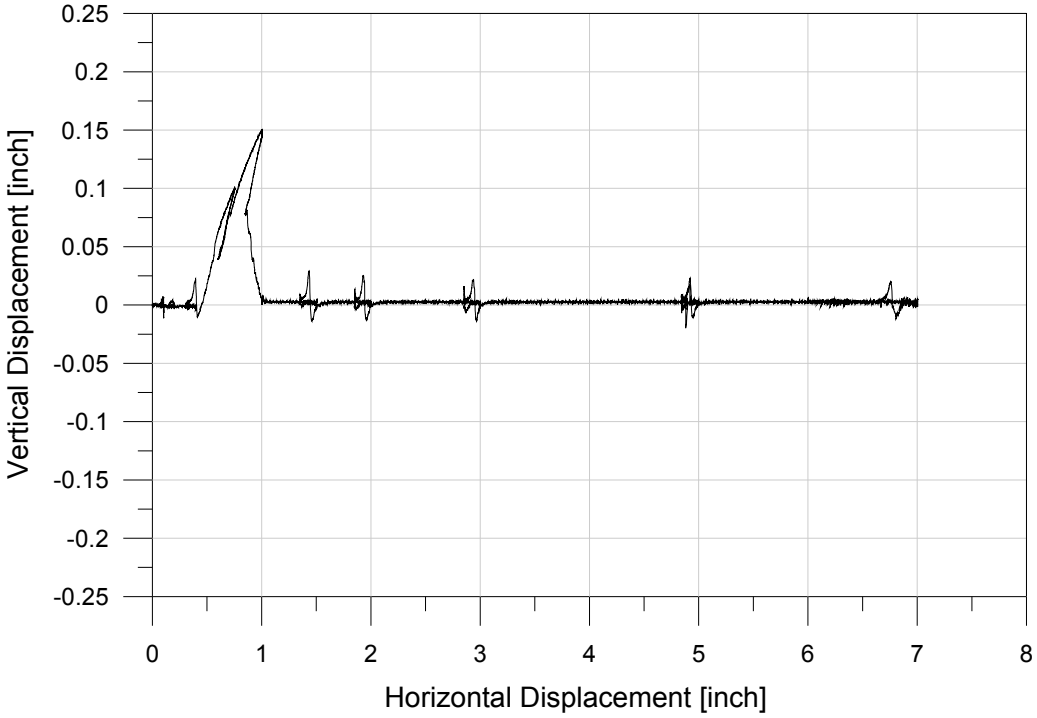

Figure 5.13.Vertical displacement (act 4) versus horizontal wall movement

The motion of the reaction block was measured with a string pot installed between the geometric centroid of the reaction block and another test specimen that was on the opposite side of the reaction block from the wall specimen (i.e., a 9 pile group with a pile cap). The original distance between the reaction block and the cap was 12.40 ft. The negative displacement indicates retraction of the string pots and consequently a movement of the reaction block towards the cap of the 9 pile group and away from the wall. The relationship between wall displacement and reaction block displacement is depicted in Figure 5.14. The reaction block movement is much smaller than the wall specimen movement.

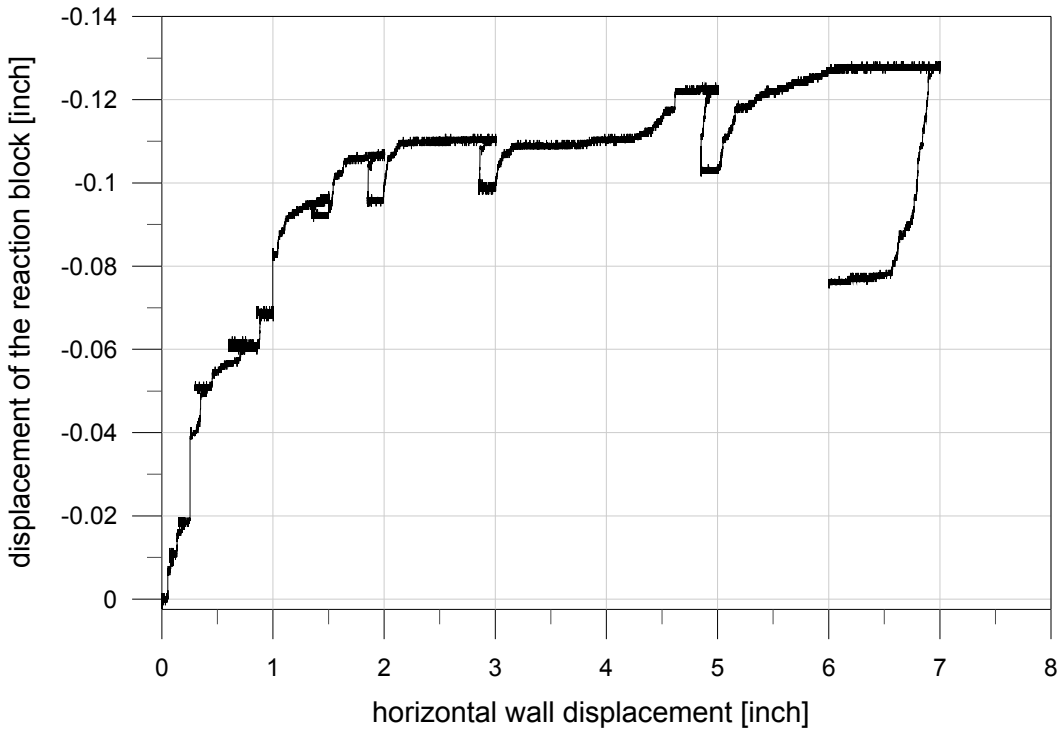

Figure 5.14. Displacement response of the reaction block

6 SOIL FAILURE INVESTIGATION

6.1 Surface Cracking Patterns

Ground surface cracking was monitored throughout the test and marked with spray paint following testing. As shown in Figure 6.1, the first observable crack opened at a displacement level of 3.0 inches. The crack formed approximately 14 ft behind the face of the wall across half the backfill width. As shown in Figure 6.2, a second large crack opened at a displacement level of 5.0 inches 17 ft behind the wall and extended over the full backfill width. This crack was later shown to be the intersection of the principal failure plane with the ground surface. As shown in Figures 6.3-6.4, numerous smaller cracks were observed near the wall face having a length of less than 5 ft. Cracking was also observed parallel to the direction of wall movement near the plywood wing walls (e.g., Figure 6.3).

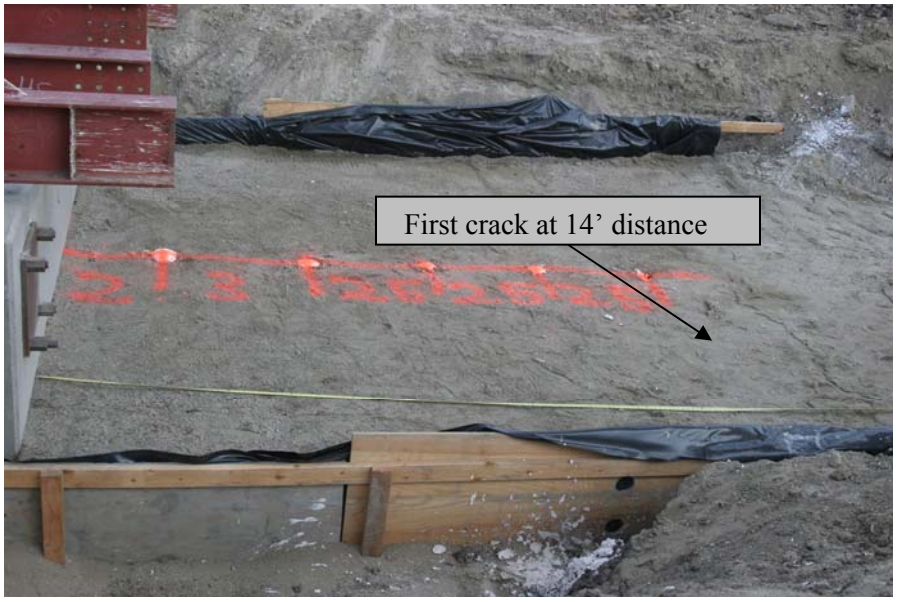

Figure 6.1. Photograph of first observable crack formation

Figure 6.2. Photograph of second crack opening at 17 feet from wall face

Figure 6.3. Photograph of crack patterns along the wall

Figure 6.4. Photograph showing surface cracks across the backfill

6.2 Trenching for Mapping of Slip Surfaces

In order to investigate the locations of subsurface cracks, low-strength gypsum columns were cast into hand-augered borehole 10 cm (4 in) in diameter. Five columns were installed at a distances of 24, 60, 90, and 120 in from the wall surface. Each column extended over the full height of the backfill and was anchored into underlying natural clay. A trench was excavated along the gypsum columns to identify depths where the columns were sheared. Table 6.1 shows the depths and shear offsets of the observed cracks and Figure 6.5 shows a photograph of the trench. As illustrated in Figures 6.6-6.7, the failure surface was found to have initiated near the base of the wall and to have reached the surface between 14 and 17 feet from the wall. The shape of the failure surface was approximately log-spiral near the wall, and it extended below the base elevation of the wall. Additional shear surfaces were observed in the columns above the principal failure plane. For example, Figure 6.7 shows a second failure surface just above the principal surface (green line). No shearing was observed in the natural soils underlying the backfill.

Figure 6.5. Exposed gypsum columns

Table 6.1. Crack locations and offsets

Gypsum Pile	*Pile 1*		*Pile 2*		*Pile 3*		*Pile 4*		*Pile 5*	
inital. dist. to wall	24"		60"		90"		120"		150"	
distance after test	23.5"		59"		89,5"		119"		148"	
	crack depth [inch]	offset [inch]	crack depth [inch]	offset [inch]	crack depth [inch]	offset [inch]	crack depth [inch]	offset [inch]	crack depth [inch]	offset [inch]
12th	4.00	0								
11th	6.00	0								
10th	12.0	0.0								
9th	18.0	-0.3								
8th	20.5	0.0								
7th	22.5	0.0								
6th	27.5	0.1	6.00	0						
5th	30.5	0.3	20.0	0.0						
4th	60.0	1.5	31.5	-0.3						
3rd	68.0	2.0	52.0	0.3	51.0	1.3			26.0	0.0
2nd	69.0	1.0	58.0	1.5	53.0	3.0			28.0	0.0
prim. Crack	71.0	2.0	67.0	4.5	62.0	2.5	44.0	4.0	32.0	4.5
clay depth	93.0		91.0				64.0		44.0	

Figure 6.6. Colored gypsum columns and corresponding offsets

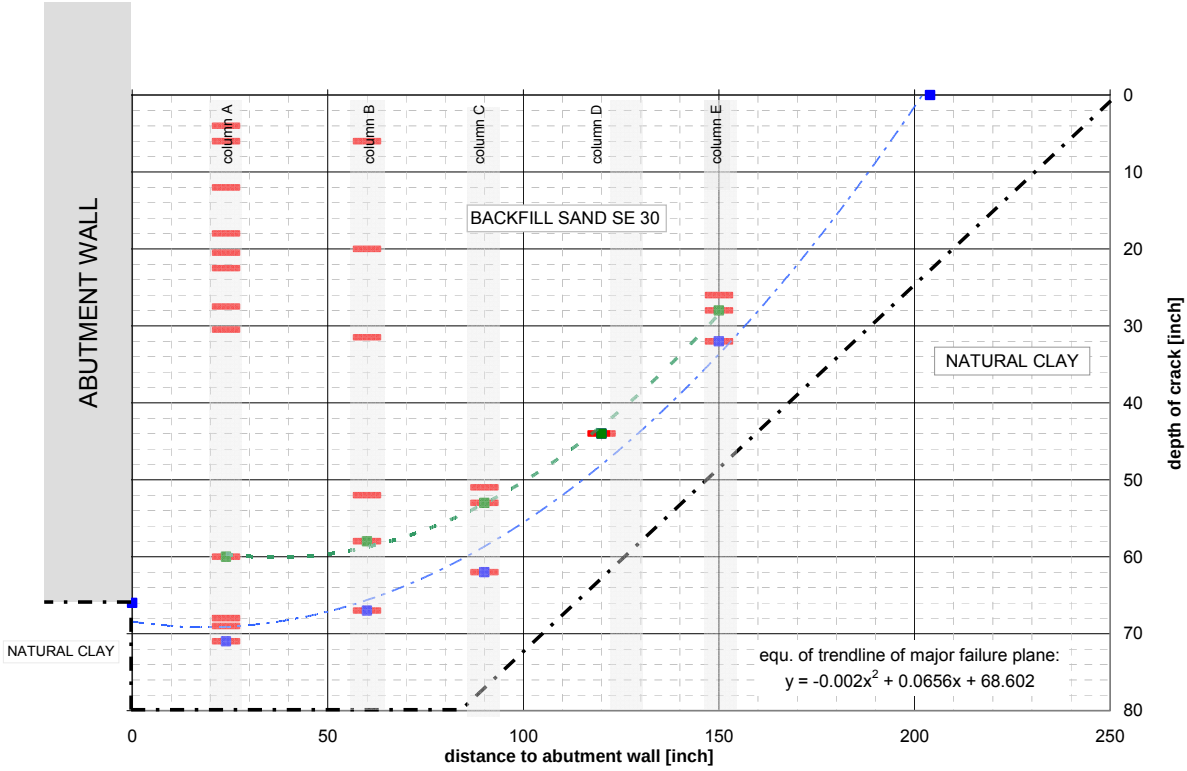

Figure 6.7. Scaled drawing of trench profile showing crack locations and failure surface

7 COMPARISONS OF TEST RESULTS TO ANALYTICAL MODELS

In this section, we compare the results of the tests to the predictions of analytical models. We focus in particular on two critical metrics of wall performance: the ultimate passive resistance and the load-deflection relationship. The properties used for the analytical predictions are as follows:

Height of backfill immediately behind wall, H = 5.5 ft (1.52m)

Width of wall, B = 15 ft (3.04m)

Drained friction angle and drained cohesion of backfill soil:

ϕ' = 40 degrees, c′ = 300 psf (14 kPa)

ϕ' = 39 degrees, c' = 500 psf (24 kPa)

Soil unit weight, γ = 127 pcf (2.04 g/cm^3)

Wall-soil interface friction angle, δ = 14 degrees

Results of the comparisons are given in Table 7.1. The Rankine and Coulomb methods clearly under-predict the observed passive capacity. The Log Spiral method over-predicts the maximum passive earth pressure. The LSH method approximates the closest capacities to the experimental measurement, while the estimate based on Caltrans seismic design guidelines is acceptable for use in geotechnical design.

Table 7.1. Comparison of measured and predicted passive force capacities

Method:	Measured	Rankine[1]	Coulomb[2]	Log Spiral[3]	M. of Slices[4]	Caltrans[5]
	cohesion c = 0.3ksf, Φ = 40					
K_p:	**17.6**	4.6	8.43	7.95	16.14	n.a.
P_p [kip]:	**506**	239	387	590	465	413
	cohesion c = 0.5ksf, Φ = 39					
K_p:	**17.6**	4.4	7.92	7.84	18.5	n.a.
P_p [kip]:	**506**	300	460	753	533	413

[1] Rankine (1857)
[2] Coulomb (1776)
[3] Log Spiral using Duncan and Mowka (2001)
[4] LSH Method by Shamsabadi et al. (2007)
[5] Seismic Design Criteria (2006)

Figure 7.1 compares the observed load-deflection relationship with predictions prepared using several models. The graph shows predictions of the Duncan and Mokwa (2001) hyperbolic model in which the model parameters K_{max}, P_{ult}, and R_f are selected using the guidelines provided by Duncan and Mokwa. Predictions of the LSH model (Shamsabadi et al., 2005, 2007) are also shown in Figure 7.1. Both models can predict the shape of the backbone curve, the major factor distinguishing LSH and Duncan and Mokwa (using the guidelines) is the passive capacity. Also shown in Figure 7.1 are two elastic-plastic load-deflection curves. The first follows the existing Caltrans Seismic Design Criteria (K_1= 20 kip/in/ft, maximum passive pressure = 5 ksf), and is shown to significantly underestimate the abutment stiffness because it is derived from previous testing using clayey backfill (Romstad et al., 1995). The second elastic-plastic curve is drawn using K_{50}=50 kip/in/ft and the same maximum passive pressure of 5.0 ksf. As shown in Figure 7.1, this provides a better fit to the data, although we note this does not represent a current design standard.

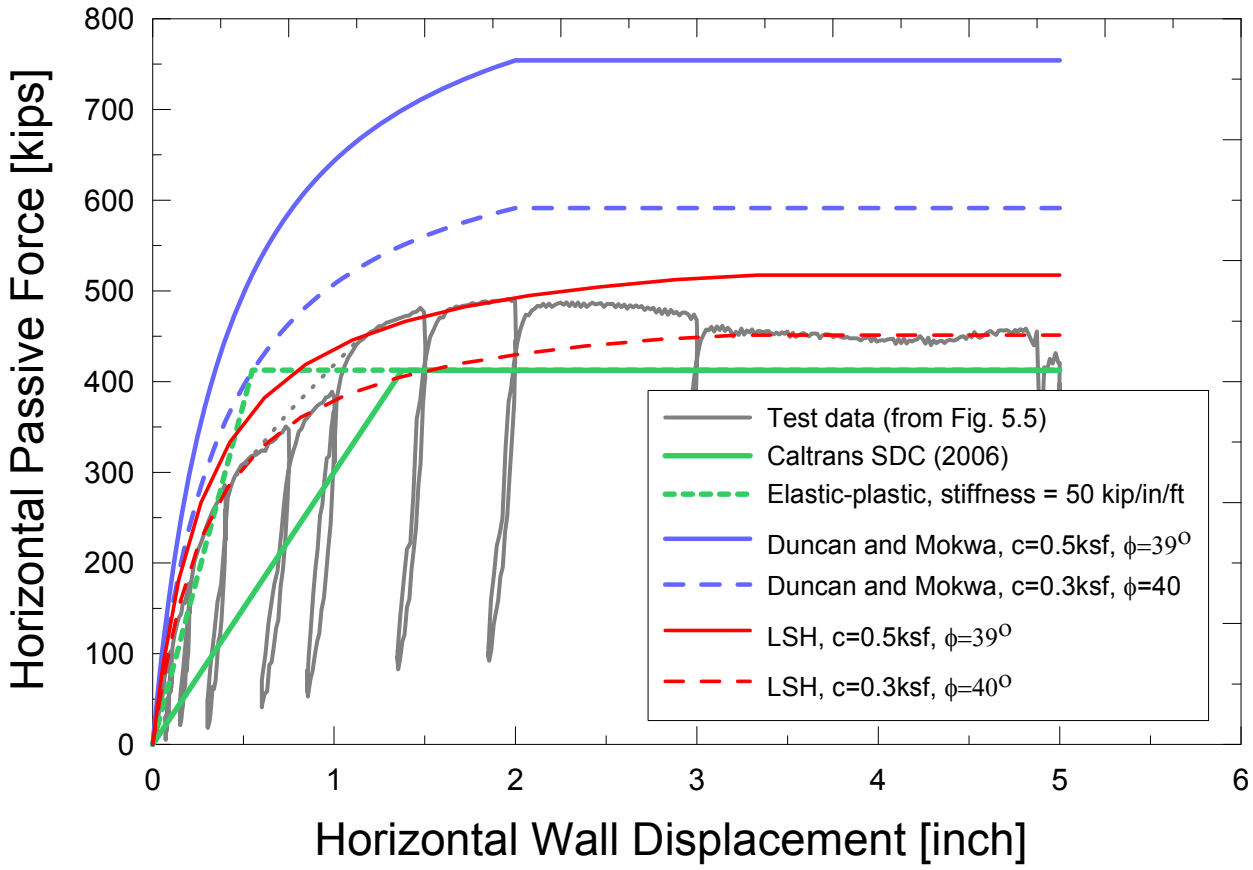

Figure 7.1. Predicted load-deflection relationships

Next, we turn to fitting hyperbolic formulations to the observed backbone curve. The fit is optimized to the residual load measured during the test in lieu of the peak. Using first the Duncan and Mokwa (2001) parameterization of the hyperbolic curve, we take parameters K_{max} and $P_{H\text{-}ult}$ as the K_i and P_p values, respectively, determined from our test data (K_i = 85 kip/in/ft, $P_{H\text{-}ult}$ = 450 kip) and R_f = 0.85 (recommended value from Duncan and Mokwa). This result, shown in Figure 7.2 proves a good match to the test data. We next fit the test data using the model formulation shown in Figure 2.6 in which y_{50} and $P_{H\text{-}ult}$ are taken directly from the test data (y_{50} = 0.33 in, $P_{H\text{-}ult}$ = 450 kip). The parameter y_{max} is taken as 0.05H (3.3 inch). The corresponding values of A and B per Eq. 2.8 are A = 0.01099 in/kip/ft and B = 0.03 in/kip/ft. Using Equations 2.6 and 2.8, the hyperbolic formulation fitting the can then be given as

$$0 < P < P_{max}: \quad \frac{P}{w} = \frac{y}{0.000733 + 0.002y}$$

$$P > P_{max}: \quad P = P_{max}, \tag{7.1}$$

where w = width of the abutment backwall.

The results of this fit are also shown in Figure 7.2.

Similar fits could readily be derived for the passive resistance at peak conditions.

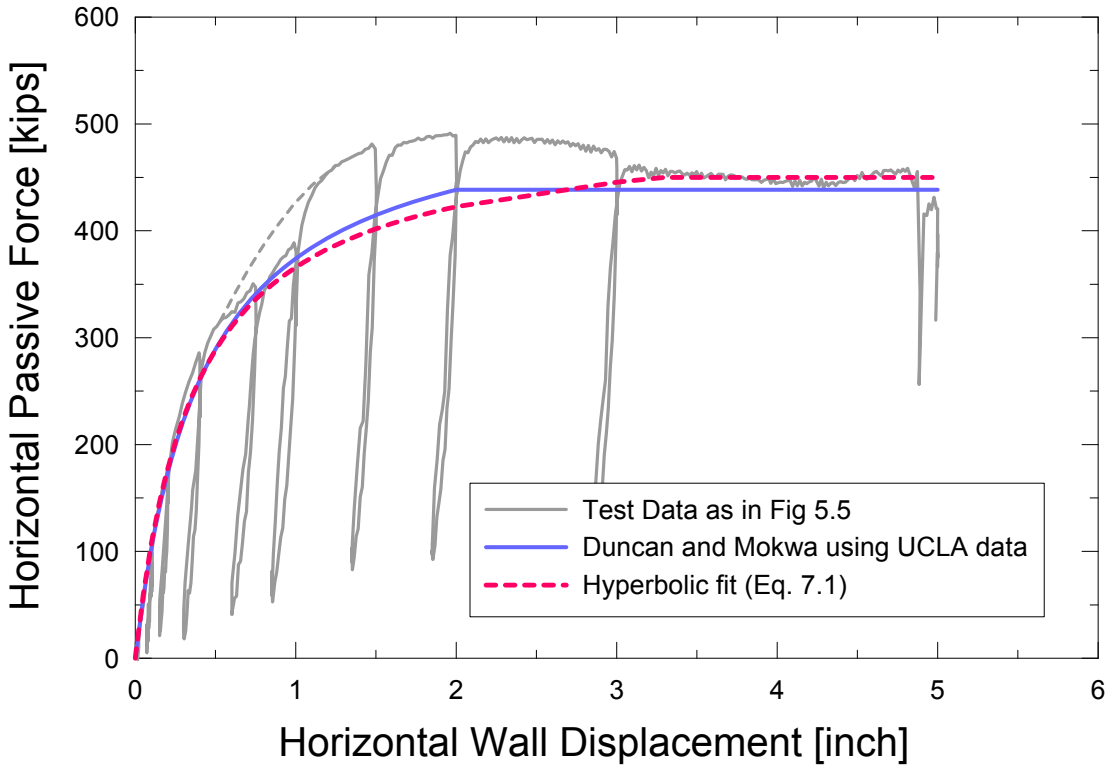

Figure 7.2. Hyperbolic fits of the backwall load-deflection relationship

8 SUMMARY AND RECOMMENDATIONS

In current Caltrans' practice (e.g., Caltrans Seismic Design Criteria, 2006), the load-deflection relationship for abutment wall-backfill interaction is described by a bilinear (elastic-perfectly plastic) model as depicted in Figure 2.7. The first parameter defines the elastic stiffness and is currently taken as 20 kips/in per foot of wall width. The second parameter defines the backfill passive capacity and is taken as a uniform pressure of 5.0 ksf acting normal to the wall. Both of these recommendations are for a 5.5 ft high wall and are derived from the results of abutment wall tests with clayey backfill soils (see Section 2.2 for details).

As described in this report, the UCLA abutment test involved a backwall 5.5 ft high with well-compacted silty sand backfill material (SE 30) that is commonly found in Caltrans' bridge abutments. The specimen was constructed and tested under boundary conditions in which the wall was displaced laterally into the backfill and not allowed to displace vertically. A maximum passive capacity of 490 kips was attained at a wall displacement of about 2.0 in, which corresponds to a passive earth pressure coefficient K_p of 17.6. Strain softening occurs following the peak resistance, and a residual resistance of approximately 450 kips is achieved for displacements > 3.0 inch. The equivalent residual passive earth pressure coefficient is K_p = 15.6 and the equivalent uniform passive pressure at residual is approximately 5.5 ksf, which is larger than the value in the 2004 Seismic Design Criteria of 5.0 ksf. The average abutment stiffness K_{50} was defined as a secant stiffness through the origin and the point of 50% of the ultimate passive force. For an abutment wall with a backfill height H of 5.5 ft, this stiffness was found to be K_{50} = 50 kip/in per foot of wall.

Based on the above results, the parameters of a bi-linear load-deflection relationship of the type shown in Figure 2.6 (which is being used for the 2006 version of the Caltrans Seismic Design Criteria) can be conservatively estimated as:

$$K_{abut} = 50\frac{kip/in}{ft} \cdot w \tag{8.1}$$

$$P_{ult} = (5.0ksf) \cdot H \cdot w \tag{8.2}$$

where H and w are the effective height and width of the abutment wall in feet, and K_{abut} is in kips/inch per foot of wall width, and P_{ult} is in kips per foot of wall width.

Hyperbolic curves provide a better representation of the load-deflection behavior of the abutment wall-backfill system than does a bi-linear relationship. Previous parameterizations of hyperbolic curves describing load-deflection behavior are given by Duncan and Mokwa (2001) and the LSH model of Shamsabadi et al. (2007), as depicted in Figures 2.5 and 2.6, respectively. A hyperbolic fit through the test data (constrained to match the residual and not the peak force capacity) was developed with the result given in Equation 7.1. Similarly, a logarithmic fit to the data can be developed, with the result given in Equation 7.2.

The mobilized wall-soil interface friction angle δ was determined as a function of displacement using the relationship between the horizontal and the vertical passive pressure resultant. The mobilized friction angle was found to vary with displacement level, with typical values in the range of 13 to 20 degrees.

Several valuable lessons were learned over the course of the testing program regarding test procedures. Critical components of the test set up that should be replicated in future tests include: (1) displacement control of the wall movement during testing that only allows displacement in the desired horizontal direction (parallel to the reaction force that would applied by the bridge deck on the backwall); (2) sand backfill must extend below the wall invert elevation to a sufficient distance behind the wall that the failure surface is entirely confined to the sand; (3) wingwalls should be simulated with suitable materials to minimize backfill displacements perpendicular to the direction of backwall movement; (4) low strength gypsum columns placed in the backfill material should be used to indicate the location of the failure surface.

Additional testing of backwall load-deflection performance is strongly recommended. The test program described in this report is an important first step, but much more work is needed to generalize the results. The results presented here apply for a single backfill height and soil condition, and for loads applied perpendicular to the wall. Many applications involve

different wall heights, different backfill materials, and walls skewed relative to the direction of the roadway (and hence the direction of the applied load). These conditions can be simulated analytically, but testing is needed to validate the results. It is also desirable to extend wall testing to dynamic loading rates that more accurately represent earthquake conditions.

References

Bowles, J.E. (1996). *Foundation analysis and design*, 5th edition, Mc Graw-Hill, New York, New York.

Bozorgzadeh,A., Ashford, S.A., Restrepo, J.I. (2006), "Effect of backfill soil type on stiffness and ultimate capacity of bridge abutments: large-scale tests," *5th National Seismic Conference on Bridges and Highways*, San Francisco, Paper No. B01

Brinch Hansen, J. (1966). "Resistance of a rectangular anchor slab,." Bull. No. 21, Danish Geotechnical Institute, Copenhagen, 12–13.

Canadian Geotechnical Society (1992). *Canadian foundation engineering manual*, 3rd edition, BiTech, Vancouver, B.C., Canada.

Carder, D.R., Pocock, R.G., and Murray, R.T. (1977). "Experimental retaining wall facility-lateral stress measurements with sand backfill," *Rep. 766, Transport and Road Research Laboratory*, Crowthorne, Berkshire, England.

Cole, R.T. and Rollins, K.M., (2006). "Passive earth pressure mobilization during cyclic loading," *J. Geotech. & Geoenv. Engrg.* ASCE, 132(9), 1154-1164.

Caquot, A. and Kerisel, J. (1948). *Tables for the calculation of passive pressure, active pressure and bearing capacity of foundations*, Gauthier-Villars, Paris.

Coulomb, C. A. (1776) "Essai sur une application des regles des maximis et minimis a quelques problemes des statique relatifs a l'architecture". Mem. Acad. Des Sciences, Paris, France.

Das, B.M. (2002) *Principles of Geotechnical Engineering*, 5th edition, Brooks/Cole, Pacific Grove, California.

Duncan, J.M., and Chang, C.-Y. (1970). "Nonlinear analysis of stress and strain in soils." *J.Soil Mech. And Found.Div.,* 96(5), 1629-1653.

Duncan, M.J. and Mokwa, R.L. (2001). "Passive earth pressure: theories and tests," *J. Geotech. & Geoenv. Engrg.* ASCE, 127(3), 248-257.

Earth Mechanics, 2005. "Field Investigations Report for Abutment Backfill Characterization, Response Assessment of Bridge Systems - Seismic, Live, and Long Term Loads." *Report to Dept. of Structural Engineering, University of San Diego, La Jolla*

Fang, Y.-S., Chen, T.-J., Wu, B.-F. (1994). "Passive earth pressure with various wall movements," *J. Geotech. Engrg.* ASCE, 120(8), 1307-1323.

Gadre, A. and Dobry, R. (1998). "Lateral cyclic loading centrifuge tests on square embedded footing," *J. Geotech. & Geoenv. Engrg.* ASCE, 124(11), 1128-1138.

Goel, R. K. and Chopra, A. K. (1995). "Evaluation of abutment stiffness in a short bridge overcrossing during strong ground shaking." *Proc. of the Fourth U. S. Conference on Lifeline Earthquake Engineering, Technical Council on Lifeline Earthquake Engineering*, Monograph No. 6, August.

James, R.G. and Bransby, P.L. (1970). "Experimental and theoretical investigations of a passive earth pressure problem," *Geotechnique*, 20(1), 17–36.

Janbu, N. (1957). "Earth pressure and bearing capacity calculations by generalized procedure of slices," *Proc. 4th Int. Conf. on Soil Mechanics and Foundation Eng.*, Vol. 2, pp. 207-213.

Lam, I. P. and Martin, G. R. (1986). "Seismic Design of Highway Bridge Foundations," Reports FMWA/RD-86/101,102, and 103, Federal Highway Administration, Washington, D.C.

Mackey, R.D. and Kirk, D.P. (1968). "At rest, active and passive earth pressures," *Proc. Southeast Asian Conf. on Soil Mech. and Found. Engrg.*, Asian Institute of Technology, Bangkok, Thailand, 187–199.

Maroney B., Romstadt K., and Kutter, B.L. (1993). "Experimental testing of laterally loaded large scale bridge abutments," *Structural Engineering in Natural Hazards Mitigation,* Proceedings, Structures Congress '93, ASCE, Irvine, CA, A. Ang and R. Villaverde (eds.), Vol. 1, pp. 1065-1070, April 19-21, 1993.

Mokwa, R.L. and Duncan, M.J. (2001). "Experimental evaluation of lateral-load resistance of pile caps," *J. Geotech. & Geoenv. Engrg.* ASCE, 127(2), 0185-0192.

Narain, R.J., Saran, S., and Nandakumaran, P. (1969). "Model study of passive pressure in sand," *J. Soil Mech. Found. Div.*, ASCE, 95(SM4), 969–983.

Ovesen, N.K. (1964). "Anchor Slabs, Calculation Methods, and Model Tests," Danish Geotechnical Institute, Bulletin No. 16, Copenhagen.

Rankine, W.J.M. (1857). "On the stability of loose earth." Philosophical transaction of the Royal Society of London.

Rollins, K.M. and Sparks, A. (2002). "Lateral resistance of full-scale pilecap with gravel backfill," *J. Geotech. & Geoenv. Engrg.* ASCE, 128(9), 711-723.

Rollin, K.M. and Cole, R.T. (2006). "Passive force-deflection relationships from full-scale tests," *5th National Seismic Conference on Bridges and Highways*, San Francisco, Paper No. B17.

Romstadt, K. , Kutter, B., Maroney, B., Vanderbilt, E., Griggs, M., and Yuk Hon Chai, Y.H., (1995). "Experimental measurements of bridge abutment behavior," *Report No UCD-STR-95-1*, University of California Davis, Structural Engineering Group.

Roscoe, K. H. (1970). "The influence of strains in soil mechanics," *Geotechnique*, 20(2), 129–170.

Rowe, P.W. and Peaker, K. (1965). "Passive earth pressure measurements," *Geotechnique*, 15(1), 57–78.

Salgado, R. (2006). *The Engineering of Foundations*, 1st edition, Mc Graw-Hill, New York, New York.

Schofield, A. N. (1961). "The development of lateral force of sand against the vertical face of a rotating model foundation," *Proc. 5th International Conf. Soil Mech. and Found. Engrg*, Paris, 479–484.

Shamsabadi, A., Ashour, M., and Norris, G. (2005). "Bridge abutment nonlinear force-deflection-capacity prediction for seismic design," *J. Geotech. & Geoenv. Engrg.*, ASCE, 131(2), 151-161.

Shamsabadi, A. and Nordal, S. (2006). "Modeling passive earth pressures on bridge abutments for nonlinear Seismic Soil-Structure interaction using Plaxis." *Plaxis Bulletin*, Issue 20, October.

Shamsabadi, A., Rollins, K.M., and Kapuskar, M. (2007). "Nonlinear soil-abutment-bridge structure interaction for seismic performance-based design," *J. Geotech. & Geoenv. Engrg.*, ASCE, 133(6), 707-720.

Shields, D.H. and Tolunay, A.Z. (1973). "Passive pressure coefficients by method of slices," *J. Soil Mech. and Found. Div*., ASCE, 99(12), 1043–1053.

Seismic Design Criteria, Caltrans. (2004) *Seismic design of abutments for ordinary standard bridges version 1.3.*

Seismic Design Criteria, Caltrans. (2006) *Seismic design of abutments for ordinary standard bridges version 1.4.*.

Terzaghi, K. (1943). *Theoretical Soil Mechanics*, Wiley, New York.

Tschebotarioff, G.P., and Johnson, E.G. (1953). "*The effects of restraining boundaries on the passive resistance of sand*," Rep. to the Office of Naval Research, Princeton Univ., Princeton, N.J.

U.S. Navy (1982). *Foundations and earth structures, design manual 7.2*, Naval Facilities Engineering Command, Alexandria, Va., 7.2-60–72.60.

Zafir, Z. and Vanderpool, W.E. (1998). "Lateral response of large diameter drilled shafts: I-15/US 95 load test program". *Proceedings of the 33rd Engineering Geology and Geotechnical Engineering Symposium*, University of Nevada, Reno, 161-176.

TABLE OF CONTENTS CHAPTER 6 – ABUTMENT BACKWALL TEST